Non-canonical Telomerase Reverse Transcriptase Controls Osteogenic Differentiation of Aortic Valve Cells Through STAT5

Rolando A. Cuevas[1], Luis Hortells[1,2], Claire C. Chu[1], Ryan Wong[1], Alex Crane[1], Camille Boufford[1], Cailyn Regan[1], William J. Moorhead III[1], Michael J. Bashline[1], Aneesha Parwal[1], Angelina M. Parise[1], Aditi Gurkar[3], Dennis Bruemmer[4], John Sembrat[5], Ibrahim Sultan[6], Thomas G. Gleason[7], Marie Billaud[8], and Cynthia St. Hilaire[1,9*]

[1] Division of Cardiology, Department of Medicine, Pittsburgh Heart, Lung, Blood and Vascular Medicine Institute, University of Pittsburgh, Pittsburgh, Pennsylvania, USA.

[2] current address - Institute for Experimental Cardiovascular Medicine, University Heart Centre Freiburg–Bad Krozingen, Medical Center and Faculty of Medicine, University of Freiburg, Freiburg, Germany.

[3] Aging Institute, Division of Geriatrics, Department of Medicine, University of Pittsburgh, Pittsburgh, Pennsylvania, USA.

[4] Department of Cardiovascular Medicine, Cleveland Clinic, Cleveland, OH, USA.

[5] Division of Pulmonary, Allergy, and Critical Care Medicine, University of Pittsburgh School of Medicine, Pittsburgh, PA, USA.

[6] Division of Cardiac Surgery, Department of Cardiothoracic Surgery, Heart and Vascular Institute, University of Pittsburgh Medical Center, Pittsburgh, Pennsylvania, USA.

[7] Division of Cardiac Surgery, Univ. of Maryland School of Medicine, Baltimore, MD, USA.

[8] Department of Surgery, Division of Cardiac Surgery, Brigham and Women's Hospital & Harvard Medical School, Boston, Maryland, USA.

[9] Department of Bioengineering, University of Pittsburgh, Pittsburgh, Pennsylvania, USA.

Running Title: TERT/STAT5 is required for cardiovascular calcification

*Corresponding Author Contact Info:
Cynthia St. Hilaire, PhD, FAHA
University of Pittsburgh
BSTWR 1744.1
200 Lothrop Street, Pittsburgh, PA 15261
+1 412-648-9441 sthilair@pitt.edu

TOTAL WORD COUNT: 5062

ABSTRACT WORD COUNT: 301

Background: Calcific aortic valve disease (CAVD) is the pathological remodeling of the valve leaflets which leads to heart failure and high stroke risk. While several mechanisms are known to drive cardiovascular calcification, the initial steps orchestrating the osteogenic reprogramming of cells are not fully understood. Non-canonical functions of telomerase reverse transcriptase (TERT) include service as a cofactor to stimulate gene transcription, and TERT overexpression primes mesenchymal stem cells to differentiate into osteoblasts. We investigated whether TERT contributes to osteogenic reprogramming of valve interstitial cells.

Methods: Baseline transcription of TERT and osteogenic markers, senescence, DNA damage, and telomere length in valve tissue and primary aortic valve interstitial cells (VICs) from control and CAVD patients were assessed. TERT expression was depleted in cells using lentiviral vectors. Cells from *Tert*$^{+/+}$ and *Tert*$^{-/-}$ mice were used to validate human findings. Immunofluorescence staining, proximity ligation assay, and chromatin immunoprecipitation assay were used in mechanistic experiments.

Results: TERT protein was highly expressed in calcified valve leaflets, without changes in telomere length, DNA damage, or senescence. These phenotypic features were retained in primary VICs isolated and cultured from those diseased tissues. TERT levels were increased with osteogenic or inflammatory stimuli, and genetic deletion or reduction of *TERT* prevented calcification of VICs isolated from humans and mice. Similar results were seen in smooth muscle cells (SMCs) and mesenchymal stem cells (MSCs). TERT and Signal Transducer and Activator of Transcription 5A/B (STAT5) colocalize and bind to the Runt-Related Transcription Factor 2 (*RUNX2*) gene promoter, and TERT and STAT5 co-localized in calcified valve tissues. Pharmacological inhibition of STAT5A prevented calcification in vitro.

Conclusions: These data show that non-canonical TERT activity is required for the calcification of VICs. TERT partners with STAT5A to bind to and activate the *RUNX2* gene promoter. These data identify a novel therapeutic target to abate vascular calcification.

ABBREVIATIONS:

αSMA, alpha 2 smooth muscle actin; VICs, aortic valve interstitial cells; CAVD, calcific aortic valve disease; ChIP, chromatin immunoprecipitation; ECM, extracellular matrix; γ-H2AX, phosphorylated gamma histone 2AX; LPS, lipopolysaccharide; BMMSCs, bone marrow mesenchymal stem cells; MSCs, Mesenchymal stem cells; NT, no treatment; OPN, osteopontin; OST, osteogenic treatment; PCNA, proliferating cell nuclear antigen; RUNX2, runt-elated transcription factor 2; STAT5, signal Transducer and activator of transcription 5A/B; TERC, telomerase RNA component; TERT, telomerase reverse transcriptase catalytic subunit; TL, telomere length; αTUB, alpha Tubulin

Key Words:

aortic stenosis, vascular calcification, calcific aortic valve disease, osteogenic differentiation, TERT, STAT

Novelty and Significance

What Is Known?

- Calcific aortic valve disease (CAVD) is the most prevalent form of aortic valve pathology. CAVD strongly correlates with age and leads to heart failure and a high risk of stroke. Currently, the only therapeutic option is valve replacement, which comes with significant healthcare costs and additional risks to patients.
- Runt-related transcription factor 2 (RUNX2) is the master transcription factor required for osteogenic differentiation of osteoblasts and osteogenic reprogramming of vascular cells, yet the early events driving its transcription in valve cells are not well defined.
- Overexpression of TERT primes mesenchymal stem cells to differentiate down the osteoblast lineage, suggesting that TERT signaling plays an important role in cell differentiation and phenotype.

What New Information Does This Article Contribute?

- TERT protein is highly expressed in calcified aortic leaflets and valve interstitial cells, independent of changes in telomere length.
- Genetic loss or depletion of TERT blocks calcification in valve interstitial cells, coronary smooth muscle cells, and mesenchymal stem cells.
- TERT co-localizes with STAT5 in the cytosol and on the *RUNX2* gene promoter, the master regulator of osteogenic transcriptional programs.

- Pharmacological inhibition of STAT5 prevents calcification of human valve interstitial cells, coronary smooth muscle cells, and mesenchymal stem cells.

What are the clinical implications?

- We have identified TERT/STAT5 as novel signaling axis that promotes the early transcriptional reprogramming in cardiovascular cells. Inhibiting TERT and STAT5 interaction and activity can be leveraged for the development of pharmacological or biological therapeutic strategies to halt or prevent calcification in the aortic valve and perhaps other cardiovascular tissues.
- Surgical procedures are currently the only treatment option for patients with CAVD. Discovering the early events driving vascular calcification identifies novel and druggable targets for the development of non-surgical therapies.

INTRODUCTION

Calcific aortic valve disease (CAVD) encompasses a spectrum of pathological remodeling of the valve leaflet, ranging from mild valve thickening that displays microcalcifications to macrocalcifications that predominate in more advanced disease stages.[1] Aortic stenosis results from fibrotic remodeling and the formation of calcified nodules on the valve leaflet that impede and disrupt blood flow, causing excessive strain on the cardiac tissue, increasing the risk of stroke, and leading to heart failure.[2] CAVD severity and incidence increase with age. CAVD prevalence rapidly increases with age and is >1,000 per 100,000 individuals ≥75 years of age.[3,4] Further, roughly 1-2% of the population harbors bicuspid aortic valve malformations, and these malformed valves are prone to calcify and develop CAVD.[5] Currently there is no therapeutic treatment that halts or reverses pathologic calcification that occurs in the valve leaflets, or other cardiovascular tissues. The only therapeutic option to treat aortic stenosis is valve replacement via surgical or transcatheter procedures, incurring substantial medical costs and health care burden to the patient.[6]

Aortic valve interstitial cells (VICs) are the primary cell type of the valve leaflet and are responsible for maintaining valvular integrity. VICs reside in a quiescent state; however, adaptive or maladaptive responses to environmental factors such as inflammation, breakdown of the extracellular matrix (ECM), and mechanical stress may disrupt VIC homeostasis.[7,8] With alterations in homeostasis, VICs acquire a myofibroblast-like phenotype, termed “activated VICs,” capable of proliferation, contraction, and secretion of proteins that further remodel the extracellular milieu.[9] Activated VICs can transition into a calcifying cell; however, how the initial steps regulating the osteogenic switching of cells are not fully understood. It is well established that the osteogenic differentiation of VICs and also vascular smooth muscle cells (SMCs) is

similar to the differentiation of mesenchymal stem cells (MSCs) into bone-forming osteoblasts; osteogenic differentiation is primarily orchestrated by Runt-related transcription factor 2 (*RUNX2*), the master transcriptional regulator of osteogenic transcriptional programs.[10-12] Other osteogenic signature markers such as osteocalcin, alkaline phosphatase, and osteopontin are also upregulated in calcifying stem and valvular cells.[9,13] While it is accepted that VICs upregulate the expression of osteogenic genes in response to stresses such as inflammation, extracellular matrix (EMC) remodeling, and mechanical stress, the causal relationship between those stresses and the initial events in the activation of osteogenic transcriptional reprogramming remains ill-defined.

The telomerase complex consists of the telomerase RNA component (TERC) and telomerase reverse transcriptase (TERT) protein, and functions to maintain chromosome telomere length and genome integrity.[14] Independent of telomerase activity, TERT also exhibits non-canonical functions. TERT can regulate gene expression and help orchestrate chromatin remodeling.[15-17] For example, TERT acts as a cofactor in Wnt-dependent promoter activation by interacting with the chromatin remodeling protein Brahma-related gene 1 (BRG1), facilitating the expression of Wnt/β-catenin target genes.[18] In a murine model of atherosclerosis TERT induced chromatin remodeling and SMC proliferation by chaperoning the retinoblastoma-associated transcription factor 1 (E2F1) binding to S-phase gene promoters.[19,20] Linking together the themes of calcification and non-canonical TERT, two contemporary studies identified that the overexpression of *TERT* primed human MSCs to differentiate down the osteogenic lineage and develop bone-like structures.[21,22] The mechanism by which TERT drives the osteogenic differentiation of human MSCs is unknown. Collectively, these studies provide strong evidence of telomerase-independent functions of TERT in altering chromatin states and regulating gene expression via various protein-protein interactions.

In this study, we tested the hypothesis that TERT contributes to the osteogenic transition of VICs. We utilized primary human aortic valve tissues from healthy control donors and CAVD patients and generated patient-specific VIC lines for in vitro disease modeling. We established baseline patterns and osteogenic induction of *TERT* and calcification markers in CAVD tissue and VICs, and assessed the consequences of genetic deletion or depletion of *TERT* during osteogenic differentiation in several cell types. We further defined the underlying mechanism by which TERT and STAT5 participate in the osteogenic transition of VICs.

METHODS

Data Availability

The Materials and Methods and the Major Resources Table are available in the Supplemental Material. The data that support the findings of this study, experimental materials, and analytic methods are available from the corresponding author upon reasonable request.

RESULTS

TERT is upregulated in CAVD valve tissue

Human aortic valves were collected after surgical aortic valve replacement procedures or from cadaveric tissue obtained via the Center for Organ Recovery and Education (CORE) of the University of Pittsburgh and processed as previously described.[23] Macroscopic examination and histological staining with Von Kossa were used to determine and confirm whether valves could be classified as a non-calcified control or as having calcific aortic valve disease (CAVD) (**Figure 1A, Supplemental Figure 1A, Table 1 and 2: Patient Information**). RUNX2 is the master transcription factor required for stem cells to differentiate into osteoblasts,[24] and is critical for the pathological osteogenic differentiation of vascular cells.[25] Immunofluorescent staining of the early calcification marker RUNX2 and the late calcification marker OPN show they were

significantly upregulated in CAVD tissue compared to control tissues, indicating activation of osteogenic transcriptional programs in CAVD tissues (**Supplemental Figure 1B**). As TERT is highly expressed in stem cells and its overexpression primes MSCs to differentiate into the osteogenic lineage,[21,22] we analyzed the expression of the *TERT* transcript and found that it was significantly upregulated in CAVD tissue relative to control samples (**Figure 1B**), and its levels positively trend with the donor's age (**Supplemental Figure 1C**). The expression of genes involved in senescence (Cyclin Dependent Kinase Inhibitor 1A (*CDKN1A*) and Galactosidase Beta 1 (*GLB1*)), proliferation (Proliferating Cell Nuclear Antigen (*PCNA*)), DNA damage (Tumor Protein 53 (*TP53*)), and cytoskeletal markers (actin Alpha 2 Smooth Muscle/αSMA (*ACTA2*); Vimentin (*VIM*)) and interleukin 6 (*IL6*) showed no differences, while the inflammatory marker and tumor necrosis factor alpha (*TNF)* was elevated in CAVD samples (**Supplemental Figure 1D**), suggesting a role for inflammatory signaling in calcification pathogenesis, as also observed by others.[26,27]

TERT protein expression and distribution was analyzed in serial sections of control and CAVD tissues. We detected an elevated TERT protein signal in CAVD valves compared to controls, with the signal localized to areas of calcification, and the number of cells expressing TERT was significantly elevated in CAVD tissues compared to non-calcified control tissues (**Figure 1C**). TERT was observed in both nuclear and cytosolic areas (**Supplemental Figure 1E).** No differences were detected in the staining levels of proliferation marker proliferating cell nuclear antigen (PCNA) or the DNA damage indicator phosphorylated gamma histone 2AX (γ-H2AX), between CAVD and control tissues (**Supplemental Figure 1F**). We found no differences in relative mean telomere length between control and CAVD tissues (**Figure 1D**), indicating similar canonical telomere extending functions of TERT in both groups. The mean age of CAVD and control patients in this study was 68 and 54 years old, respectively (**Figure 1E**). Together, these

data show that TERT, osteogenic markers, and inflammatory signatures are upregulated in CAVD tissue while markers indicating alterations in proliferation, DNA damage, and senescence are not altered in CAVD leaflets. Importantly, despite the elevated TERT expression and protein levels, telomere length remains unaltered between CAVD and control tissue, suggesting non-canonical TERT activity.

CAVD in vitro disease modeling with VICs recapitulates in vivo observations

We created patient-specific VIC lines isolated from CAVD and control valves.[23] At baseline, VICs freshly isolated from CAVD and control patients exhibited no morphological, proliferative, or migratory differences (**Figures 2A, 2B**, **2C**, **and Supplemental Figure 2A,** respectively) while TERT and RUNX2 proteins were significantly elevated in CAVD VICs (**Figure 2D**). At baseline, we observed no differences between CAVD and control VICs in SM22 or αSMA — markers of an activated VIC phenotype (**Supplemental Figure 2B**)— but found significantly higher levels of the mineralizing enzyme tissue non-specific alkaline phosphatase (TNAP) in CAVD VICs (**Supplemental Figure 2C**). Like in the leaflet, there was no difference in the mean telomere length between CAVD and control groups (**Figure 2E**). Thus, these data show that at baseline, VIC isolated from CAVD patients display elevated TERT and RUNX2 expression, recapitulating the osteogenic phenotype observed in CAVD leaflet tissue, and confirming the telomere activity of TERT is not operative in these established cells lines.

TERT expression is upregulated in VICs under osteogenic conditions

To model CAVD disease in vitro and establish a role for TERT during VIC osteogenesis, we cultured CAVD and control VICs in osteogenic media conditions (OST, see Methods Section), a media widely utilized to induce osteogenic differentiation of osteoblasts.[28] Calcification was visualized using Alizarin Red stain and revealed that OST-treated CAVD and control VICs lay

down calcified matrix as early as 14 days (d14), and CAVD VICs calcified earlier relative to control VICs under the same conditions. Importantly, we observed that CAVD VICs calcify de novo under no treatment (NT) conditions, suggesting that CAVD VICs are primed for osteogenesis (**Figure 3A**). Protein analysis revealed increased levels of TERT in control VICs at d14 of OST treatment, while in CAVD VICs TERT was elevated under NT conditions, suggesting that TERT has an active role in the osteogenesis of VICs. The calcification markers RUNX2 and OPN were upregulated indicating active osteogenesis (**Figure 3B**). Immunofluorescent staining of VICs showed that at d14 under NT conditions, TERT was elevated in CAVD VICs relative to control VICs (**Figure 3C**, left panels) and that TERT signal was intensified on d14 of OST treatment (**Figure 3C**, right panels). While both control and CAVD VICs exhibit calcification on d14, CAVD VICs form larger calcified nodules (**Figure 3C**, right panels), and we observed no differences in cell numbers at the end of the 14-day assay under NT or OST treatment conditions (**Supplemental Figure 3A**). Transcriptional analysis showed that the osteogenic markers *BMP2*, *THBS1*, *ALPL;* myofibroblast markers *CNN1*, *TAGLN*, *SMTN;* calcification-associated gene *FOXO1;*[29] and the CAVD-associated metalloproteinase *MMP13*[30] were significantly upregulated in control VICs at d14 of OST treatment. We also found significant upregulation of the pro-inflammatory transcription factor Signal Transducer and Activator of Transcription 5A *(STAT5A)* gene while the expression of the isoform *STAT5B* gene remained unchanged (**Figure 3D**). These results confirmed that VICs undergo osteogenesis as opposed to de novo mineral nucleation.[31]

In cancer and stem cells, the enhanced canonical activity of TERT leads to long telomeres and enables unlimited proliferation,[32] while short telomeres can trigger cellular senescence.[33] Although we observed no differences in telomere length (**Figure 1D and 2E**), we assessed cellular senescence. We observed no differences in the expression of senescence-associated

β-galactosidase (SA-β-gal, *BGLAP*) between CAVD and control VICs at baseline **(Supplemental Figure 3B)**, or during osteogenic treatment (**Figure 4D**). We further assessed cellular senescence by senescence-associated β-galactosidase activity assay. We found that the osteogenic treatment did not trigger cellular senescence even after 28 days (**Supplemental Figure 3C**). These data confirmed that cellular senescence is not operative during the VIC osteogenesis.

TERT is required for in vitro calcification

Previous studies have shown that the overexpression of TERT primes human MSCs (hMSCs) to differentiate into osteoblasts.[21,22] To determine whether TERT is required for the calcification of human VICs, we transduced these VICs with a lentivirus expressing an shRNA targeting *TERT*. Knockdown of *TERT* caused inhibition in the calcification of VICs relative to VICs transduced with a scramble shRNA control, and downregulation of RUNX2 in human VICs (**Figures 4A and 4B**). Next, we assessed whether inhibition of the canonical telomere extending activity of TERT altered calcification of VICs. Cells under OST treatment were given the inhibitor BIBR1532, which blocks the reverse transcriptase activity of TERT, required for telomere extension.[34] A 28-day OST assay treatment with BIBR1532 did not alter the calcification of VICs (**Figure 4C**), suggesting that the canonical telomere-extending function of TERT is not required during VIC osteogenesis. Next, we assessed whether TERT was involved in the osteogenic reprogramming of other cell types. In human coronary artery smooth muscle cells (CASMCs), knockdown of TERT also inhibited calcification (**Figure 4D**). To validate these findings and confirm a broader role for TERT in osteogenic differentiation, we investigated TERT's effect in human MSCs. Human MSCs exhibited robust calcification as early as day 14 of the OST treatment, while cells in NT conditions did not calcify (**Supplemental Figure 4A**). Protein analysis showed TERT protein level increases on day 3 of the OST differentiation, coinciding

with the increase in *RUNX2* expression and RUNX2 protein levels (**Supplemental Figures 4B and 4C**). Like human VICs, human MSCs in OST treatment exhibited intense TERT staining, and TERT-positive cells clustered around calcified nodules (**Supplemental Figure 4D**). As in our previous assays, the knockdown of *TERT* inhibited calcification of human MSCs (**Supplemental Figures 4E and 4F**). Together, these data suggest that TERT is required for the osteogenic differentiation of human VICs, CASMCs, and MSCs.

To further confirm our findings that TERT is required for calcification, we utilized a genetic approach. Murine VICs (mVICs) and bone marrow MSCs (mBMMSCs) were isolated and expanded from *Tert*-knockout (*Tert*$^{-/-}$) and wild-type (*Tert*$^{+/+}$) mice.[35] *Tert*$^{-/-}$ mice were generated from heterozygous breeding pairs (F1 generation) and thus do not exhibit shortened telomeres.[36] In support of our findings in the human cells with depletion of *TERT*, we found that deletion of *Tert* drastically inhibited calcification of mVICs and mBMMSCs compared to *Tert*$^{+/+}$ cells, which exhibited robust calcification, as revealed at d21 of OST treatment by Alizarin Red staining (**Figures 5A and 5B**). Notably, TERT deficiency or OST treatment did not induce senescence in mice *Tert*$^{-/-}$ cells as determined by SA-β-gal activity (**Supplemental Figures 5A and 5B**). Together, these data show that TERT is required for the osteogenic transition of mice VICs and BMMSCs, and that senescence is not operative during the osteogenic differentiation of murine cells.

TERT Interacts with STAT5 to bind the *RUNX2* gene promoter

TERT exerts transcriptional gene regulation in various tissues and cells by physically interacting with transcription factors such as NF-κB, Sp1, and E2F1.[17,20,37,38] Increased RUNX2 expression and activity is the hallmark of osteoblast differentiation and vascular calcification.[25] RUNX2 is the master regulator of osteogenic differentiation and we found that RUNX2 is downregulated in

TERT-knockdown cells (**Figure 4**). We used the LASAGNA[39] and TRANSFAC/MATCH[40] programs to identify putative transcription factor binding sites in the 5kb region upstream of the human *RUNX2* gene promoter (NM_001015051.3) and identified 13 potential STAT5 binding sites (**Table 2**). We observed increased expression of *STAT5A* during the osteogenic differentiation of VICs (**Figure 3D**). Two different genes encode STAT5A and STAT5B, but 96% of their amino acid sequence is shared and their activities redundant; herein we refer to both genes as STAT5 when available tools (e.g. antibodies) do not allow for isoform differentiation.[41] We found that OST treatment upregulated STAT5 protein in VICs, and STAT5 was detected in the nucleus of OST-stimulated VICs (**Supplemental Figures 6A and 6B**). Next, we utilized proximity ligation (PLA) to examine TERT and STAT5 colocalization, as this technique is capable to detect interacting proteins in a proximity range below 40 nm. PLA revealed that TERT and STAT5 significantly colocalized in control VICs after 21 days of OST treatment (**Supplemental Figure 6C**). Likewise, TERT/STAT5 colocalization was elevated in CAVD VICs after 21 days of OST treatment compared to control VICs (**Figure 6A**). We next sought to determine whether TERT and STAT5 are bound to the *RUNX2* gene promoter region. We identified 13 potential STAT5 binding sites (**Table 2**) and focused on sites -1371 bp and -193 bp upstream of the start site as both have high homology to the tetrameric consensus STAT5 binding site and show an elevated likelihood of being functional sites (core and matrix scores of 0.788 and 0.834, and 0.995 and 0.882, respectively, **Figure 6B**). Chromatin immunoprecipitation analysis (ChIP) in control VICs shows that STAT5 binds to the *RUNX2* promoter at both sites, and that the binding enrichment was significantly higher during osteogenic differentiation (**Figure 6C**). While we found that TERT also binds to -1371 bp and -193 bp of RUNX2 promoter, the trending enrichment during OST treatment did not reach statistical significance, perhaps suggesting that TERT itself does not bind to DNA directly but sits alongside STAT5 on the *RUNX2* gene promoter.

We utilized a pharmacological approach to identify whether one or both STAT5 proteins contribute to osteogenic reprogramming. We treated human VICs with the small molecules StafiA-1 and StafiB-1, which have been reported to specifically inhibit STAT5A and STAT5B, respectively.[42,43] We found that StafiA-1 significantly inhibited calcification of VICs during a 21 days OST assay and that this inhibition was of a greater extent than the inhibition observed when VICs were treated with StafiB-1, suggesting that STAT5A is the main participant during the osteogenic reprogramming of VICs (**Figure 6D**). Similarly, we found that StafiA-1 significantly reduced the calcification in human CASMCs and MSCs while StafiaB-1 did not (**Supplementary Figures 6D and 6E**). Together, these data show that TERT and STAT5A interact to localize STAT5A to its cognate sites in the *RUNX2* promoter to drive osteogenic transcriptional reprogramming.

We explored the mechanism by which TERT and STAT5 become activated during the osteogenic differentiation of human VICs. As inflammation contributes to CAVD pathogenesis,[44] we used bacterial lipopolysaccharide (LPS) to trigger inflammatory response pathways in VICs[45] and found that LPS was sufficient to induce calcification of VICs. Like OST treatment, TERT-positive cells accumulated near calcified nodules after LPS and osteogenic stimulation (**Supplementary Figure 6F**). Protein analysis showed that LPS alone was also sufficient to upregulate TERT, RUNX2, and STAT5 proteins (**Supplementary Figure 6G**). Together, these observations indicate that LPS/TLR4 inflammatory signaling pathway participates in the regulation of TERT and the osteogenic transition of human VICs.

TERT and STAT5 are upregulated in CAVD tissue

Our data illustrate a requirement of TERT for calcification and show TERT/STAT5A drives osteogenic reprogramming by binding to the *RUNX2* gene promoter. To confirm the role of these proteins in vivo, we quantified the staining of TERT and STAT5 in human valves. We found that STAT5 protein is highly expressed in the CAVD leaflet and localized to areas of calcification, mirroring TERT distribution in the valve leaflet, while the number of STAT5-positive cells was significantly increased in CAVD tissue (**Figure 7A**). Furthermore, STAT5 highly colocalized to TERT-positive cells in the valve (**Figure 7B**). Altogether, these data support our in vitro investigations and suggest that TERT contributes to CAVD pathogenesis via its interaction with STAT5A.

DISCUSSION

This study reveals a novel mechanism for TERT in driving a human pathology (**Figure 8**). These data establish that TERT is upregulated in CAVD tissue and in primary cell lines derived from those tissues, and that TERT is required for the osteogenic transition of vascular cells. The mechanism by which TERT promotes the osteogenic reprogramming of VICs is via interaction with STAT5, and this complex binds to the *RUNX2* gene promoter. Depletion of TERT or pharmacological inhibition of STAT5 blocked calcification in vitro, and TERT/STAT5 puncta were observed on CAVD but not control human aortic valves. Collectively, these experiments support a novel role for TERT and STAT5 in driving CAVD pathogenesis and identify a unique, druggable target for cardiovascular calcification.

TERT is well-known for its canonical, telomere-extending activity, yet TERT also regulates gene expression and chromatin remodeling independent of affecting telomere integrity. For example, previous reports have shown that TERT interacts physically with several transcription factors to

promote the expression of several genes, including β-catenin to stimulate genes involved in bone development.[15,16,37] In the vasculature, TERT binds to the transcription factors SP1 at the *VEGF* promoter and E2F1 at *MCM7*, *CCNA1*, and *PCNA* promoters, stimulating SMC proliferation and neointima formation.[20,35,38,46] In this regard, we did not detect proliferative or migratory differences between control and CAVD VICs despite elevated levels of TERT at baseline (**Figures 2B and 2C**).

In addition to supporting transcription factor function, TERT also acts as a cofactor to orchestrate chromatin remodeling machinery. TERT serves as a chaperone to facilitate the recruitment of BRG1 and histone acetyltransferases to stimulate chromatin accessibility and transcription or to maintain heterochromatin structure.[18,47,48] Loss of TERT abrogates the cellular response to DNA double-strand breaks and alters the overall chromatin configuration, without affecting the short-term telomere integrity.[17] These data strongly support the prominent role of non-canonical functions of TERT. We found that TERT interacts with STAT5 and together, are recruited to two consensus sites in the *RUNX2* gene promoter during osteogenic reprogramming of VICs. Our observations that TERT is upregulated in CAVD tissue and during VIC osteogenesis support this hypothesis. Furthermore, our findings that *TERT* depletion reduced RUNX2 expression and calcification in several cell types, along with the finding of others that *TERT* overexpression drives osteogenesis in human MSC,[21,22] support a general role for TERT modulating cellular phenotypic transition and osteogenic reprogramming. From the studies mentioned above, one can speculate that perhaps TERT serves as a co-factor bridging chromatin remodeling complexes and transcription factors to facilitate euchromatin stability.

Cell replication progressively shortens telomeres, triggering senescence, yet telomere length varies widely between people of the same age.[49] Telomere length is considered a biomarker of aging, and several studies have utilized circulating leukocytes to investigate whether shortened telomeres correlate with various vascular disease states.[50,51] One study correlated circulating leukocytes as surrogates to interrogate the telomere length of patients diagnosed with CAVD featuring aortic stenosis and found that CAVD leukocytes had slightly shorter telomeres than age-matched healthy controls.[52] However, telomere length in leukocytes is not indicative of global telomere length, telomerase complex activity, or TERT protein function in all cell types. First, short telomeres may reflect increased circulating leukocyte turnover due to systemic inflammation, as leukocytes are highly proliferative. Second, telomere attrition might be a tissue- and disease-dependent process. Third, these correlative studies show no clear evidence of a causal link between telomere length, non-canonical TERT activity, and disease progression. In this regard, Huzen et al. compared the telomere length of the leukocytes of age-matched healthy controls and patients with atherosclerosis as well as the telomere length of the cells in the atherosclerotic plaques of the patients. They found that while telomere length in leukocytes from the atherosclerosis patient group was significantly shorter than in the control group, telomere length in the atherosclerotic plaques was significantly longer, indicative of increased telomerase activity.[53] Thus, total leukocyte telomere length does not represent telomere length in the diseased tissue itself. Our approach examined TERT protein expression directly in the valve tissue and in patient-specific VICs. With these tools, we determined that the expression levels of TERT and osteogenic markers in CAVD tissue were elevated, without changes in telomere length, proliferation, and DNA damage markers; thus, suggesting a non-canonical role for TERT in these cells.

VIC calcification shares aspects of the transcriptional program observed during the differentiation of MSCs into osteoblasts, including the upregulation of *RUNX2, BGLAP, TNAP*, and the secretion of bone-forming proteins and accumulation of calcium minerals.[5,10,12] Likewise, mechanical stress, disturbed flow, and inflammation promote VIC calcification, as well as the osteogenic differentiation of MSCs.[54] These observations suggest that VICs switch from their quiescent state and undergo an osteogenic transition like MSCs, acquiring osteoblast-like phenotypic features. The mechanisms driving these cell transitions are not fully understood. We have hypothesized that fully differentiated cells can de-differentiate into a transitory, multipotent stem cell-like state and then acquire an osteogenic phenotype.[55] VICs have the potential to differentiate into the osteogenic, chondrogenic, or adipogenic lineage, properties comparable to mesenchymal stem cells.[56] We focused on TERT as it is highly expressed in stem cells and its overexpression primes mesenchymal stem cells into the osteogenic lineage.[21,22] Thus, we propose that the upregulation of TERT leads healthy VICs to undergo a de-differentiation process, likely to involve broad chromatin remodeling and that in an inflammatory milieu, TERT and STAT5A couple to drive the osteogenic transition of VICs.

The osteogenic differentiation of stem cells is orchestrated by RUNX2, which is also detected in the osteogenic reprogramming of vascular cells.[25,57] In a recent transcriptomic study Xu et al. identified 14 cell populations present in aortic valve tissue samples from two healthy and four CAVD valves.[58] CAVD was diagnosed via ultrasound imaging, which detects leaflet mobility, however examining the macroscopic pictures and histological staining of valve leaflets used in this analysis shows that while these valves are indeed stiff, they do not exhibit robust nodules of calcification as do the valves in our data set (**Figures 1A, 1C, 5, and Supplemental Figure 1A**). Their analysis identified three VIC populations defined by expression of *FOS, HSPA6, SPARC.* However, cells from six valves were pooled, with 10.4% of cells coming from control

tissue and the remaining 89.6% from CAVD tissues. Bulk transcriptomic data from these tissues show only a small 1.49-fold increase in *RUNX2* gene expression in CAVD tissues, in stark contrast with our observations regarding RUNX2 expression (**Figures 1-3**) and what is currently accepted.[10-12] Inspection of the publicly available bulk RNA-sequencing data (PRJNA552159) did not show any increase in *TERT* transcript expression. While hemodynamic data showed those valves had indeed undergone fibrotic remodeling, only a low number of calcifying cells were present, as confirmed by their histological staining. This lack of calcification may explain why *TERT* expression was undetected in their study. In our study, a portion of each patient valve was used for cell isolation while the rest was utilized for calcification assessment by histological staining, following a workflow that we developed that guarantee that cells isolated from surgically removed and postmortem tissues retain their proliferative capacity and endothelial and interstitial phenotypes in culture.[23]

The function of STAT5 in bone formation is multifaceted. While it was shown that STAT5 can promote the differentiation of MSCs into osteoblasts by upregulation of the osteogenic genes in a Jak2-dependent manner,[59] a *Stat5a* global knockout mouse exhibited elevated bone mass and bone mineral density.[60] These conflicting reports indicate that the role of STAT5 in bone formation and remodeling is complex and more studies are required. STAT5 has diverse functions as a transcription factor: it interacts with histone acetyltransferases and transcription factors such as the glucocorticoid receptor, SP1, YY1, and C/EBPβ to stimulate gene expression,[61-63] and two studies in cancer cells identified that STAT5 induces *TERT* expression.[64,65] We found multiple putative STAT5 binding sites in the *RUNX2* promoter region and provide strong evidence in support of a novel mechanism in CAVD pathogenesis where TERT/STAT5 co-localize, translocate to the nucleus, and activate osteogenic gene transcription which drives the early events in cellular osteogenic transition.

While our results are robust, it is important to address the limitations of our study. STAT5A and STAT5B are two different genes with 96% of their amino acid sequence shared and their activities redundant.[41] We have determined that VICs express both variants, however, our antibodies could not differentiate between the two variants, thus it is possible that only one isoform interacts with TERT to bind the *RUNX2* gene promoter. STAT5 is activated by multiple cytokines, including IL-2, IL-6, and TNF-α,[66] and it was shown that IL-2 specifically activates STAT5 to induce TERT expression in cancer cells.[64] Whether STAT5 first induces TERT expression, and then TERT and STAT5 together cooperate to control the expression of RUNX2 needs to be determined. There is also redundancy regarding STAT1/3/5 functions and signaling.[67] Our study was not designed to address all the complexities of STAT signaling per se but rather to investigate the role of TERT utilizing STAT5 as a DNA transcription factor binding partner to activate an osteogenic transcriptional program; our future studies will investigate the role of STAT5 further.

Our work highlights the importance of primary human tissue-based studies. Murine models are not ideal to study non-genetic drivers of CAVD, as mice do not develop CAVD de novo.[68,69] Mouse leaflets' structure differs from human leaflets as they lack a trilaminar organization and present a melanocyte cell population.[70-72] Recent elegant work from the Giachelli group showed that in mice, calcification happens in the sinus wall and to a lesser extent, at the leaflet hinge, the region between the leaflet VICs and SMCs of the aorta, with no detectable calcification in the leaflets after 26 weeks of a high-fat diet in a *LDLR* knockout mice model.[73] This distribution is similar to the atherosclerotic calcification observed of the aortic root, and it is also found in a work from the Kobuta group, which detected calcification in the sinus wall after 16 weeks of valve mechanical injury.[68] Therefore, mice models do not fully recapitulate calcification or

505 pathogenesis of CAVD in humans in terms of leaflet remodeling and calcification; as such,
506 murine-based studies may not be ideal models for studying human valve disease, positioning
507 human-based studies as imperative to understand and solve the pathologic calcification of the
508 valve tissue.
509
510 We have identified a novel and innovative mechanism that contributes to CAVD pathogenesis
511 by determining a causal link between TERT and the osteogenic differentiation of valve cells.
512 This study is the first to suggest that a non-canonical function of TERT is operative in CAVD
513 pathogenesis as we did not detect telomere length differences in our specimens and the cell
514 lines established out of them. TERT was detected in the cytosol and nuclei of cells, its
515 expression was required for calcification of several cell systems, and we detected TERT bound
516 to the *RUNX2* promoter region, dynamically changing its binding during osteogenic
517 differentiation of VICs, suggesting an active non-canonical role as a STAT5-binding partner.
518 Current CAVD therapies are surgical, limited to either mechanical or bioprosthetic valve
519 replacement, and performed only when the disease has progressed to the advanced point of
520 affecting blood flow and heart function. As TERT and STAT5 become important targets in
521 cancer therapy, we propose these novel targets may perhaps be leveraged to tackle
522 calcification disease progression. Studying the disease mechanisms and effects of TERT and
523 STAT5 interaction in the context of maladaptive dysregulation in the vessels could also better
524 inform us of potential drugs to disrupt their interaction and prevent, or even reverse CAVD.
525

526 **ACKNOWLEDGEMENTS**

527 We would like to acknowledge and thank the Center for Organ Research and Education for their
528 help and support and thank tissue donors and their families for making this study possible. We
529 would also like to thank Kristin Konopka, tissue bank coordinator at The Department of

Cardiothoracic Surgery, UPMC. We would like to thank Jason Dobbins for his insightful discussion and critical reading of this manuscript.

SOURCES OF FUNDING

This study was supported by funds from the National Institutes of Health (R01 HL142932, St. Hilaire) and the American Heart Association (20IPA35260111, St. Hilaire; 902641, Cuevas).

DISCLOSURES

The University of Pittsburgh has filed a provisional patent application on behalf of CSH and RAC regarding technology based on findings presented in this manuscript. IS receives institutional research support from Atricure and Medtronic and serves as a consultant for Medtronic Vascular. None of these conflicts of interest are related to this work. All other authors have nothing to disclose.

FIGURE LEGENDS

Figure 1. TERT is upregulated in CAVD valve tissue.

A, Surgically removed specimen of control (top) and CAVD (bottom) human valves. B, TERT mRNA transcript quantification in control and CAVD valve tissues. n = 8 control, n= 9 CAVD. C, Representative serial sections of Von Kossa (dark precipitation, top panels) and TERT immunofluorescent staining (bottom panels) in control and CAVD valve tissues. Scalebar 100 µm. Quantification of TERT intensity and the number of TERT-positive cells on the leaflet is shown on the right graphs. n = 9 control, n = 9 CAVD. D, Telomere length measurements in valve tissues. n = 16 control, n = 10 CAVD. E. Age of the patients utilized in this study. n = 25 control, n = 16 CAVD. Data are shown as means ± SD. *P* values were calculated by the Mann-Whitney *U* test and shown on each graph.

Figure 2. Valve interstitial cells isolated from CAVD patients show elevated TERT expression at baseline.

A, Representative images showing cell morphology of control (left) and CAVD (right) VICs. Scalebar 50 µm. B, Proliferation of control and CAVD VICs at baseline. n = 3 control, n = 3 CAVD. Data represents means ± SD. C, Relative migration distances of control and CAVD VICs. n = 10 control, n = 10 CAVD. Representative western blot staining of control and CAVD VICs at baseline. Quantification of protein levels is shown on the right panels. n = 4 control, n = 4 CAVD/. E, Telomere length measurements in VICs. n = 8, control, n = 5 CAVD; means ± SD. Data are shown as means ± SD. *P* values were calculated by the Mann-Whitney *U* test and shown on each graph.

Figure 3. TERT is upregulated during osteogenic differentiation of VICs.

A, Representative images of VICs growing in normal conditions (no treatment, NT, left panel) or stimulated with osteogenic media (OST) for 14 days. Calcium deposition was visualized by Alizarin Red staining. Scalebar 50 µm. Quantification of calcification is shown as average absorbance ± SD on the right graphs. n = 7 control, n = 7 CAVD. B, Representative western blot staining of samples from control and CAVD VICs after 14 days of NT or OST. Quantification of protein levels is shown on the right graphs. n = 4 control, n = 4 CAVD. C, Representative immunofluorescent staining images of TERT in control and CAVD VICs after 14 days of NT or OST. Calcium deposition was visualized by OsteoImage staining. Scalebar 100 µm. D. Expression profile control VICs after 14 days of NT and OST treatment. n = 4 NT, n = 4 OST. Data are shown as means ± SD. *P* values were calculated by the Mann-Whitney *U* test with * *P* = 0.0286 in Figure D.

Figure 4. TERT is required for osteogenic transition and calcification of human cells.

A, VICs transduced with lentivirus containing either short hairpin scramble (shControl-GFP) or short hairpin TERT (shTERT-GFP) and followed by OST stimulated for up to 28 days. Calcium deposition was visualized by Alizarin Red staining. Quantification of calcification is presented as average absorbance on the right graph. n = 6 shControl, n = 6 shTERT at 21 days and n = 9 shControl, n = 9 shTERT at day 28. Scalebar 400 μm. Data are shown as means ± SD. B, Representative western blot staining of VICs transduced with lentivirus containing either shControl-GFP or shTERT-GFP followed by 7 days of osteogenic stimulation. C. VICs treated with BIBR1532 and stimulated with osteogenic media for 28 days. Scalebar 50 μm. Quantification of calcification is shown on the right graph. n = 6. Data are shown as means ± SD. D, CASMCs transduced with lentivirus containing either shControl-GFP or shTERT-GFP and stimulated with osteogenic media for up to 21 days. n = 4 shControl, n = 4 shTERT for both time points. Scalebar 400 μm. Quantification of calcification is shown on the right graph. *P* values were calculated with the Kruskal-Wallis *H* test with Dunn post hoc test and shown on top of each graph.

Figure 5. TERT is required for the osteogenic transition of murine cells.

A, Representative images of mVICs isolated from wild-type (*Tert* $^{+/+}$) or F1 Tert knockout (*Tert* $^{-/-}$) mice and stimulated with osteogenic media for 21 days. Scalebar 100 μm. Quantification of calcification is shown on the right graph. B, Representative images of mBMMSCs isolated from *Tert* $^{+/+}$ or *Tert* $^{-/-}$ mice and stimulated with osteogenic media for 21 days. Scalebar 100 μm. Quantification of calcification is presented as average absorbance on the right graphs. All graphs are n = 4 *Tert* $^{+/+}$, n = 4 *Tert* $^{-/-}$. Data are shown as means ± SD. *P* values were calculated by the Mann-Whitney U test and indicated on each graph.

Figure 6. TERT and STAT5 interact to upregulate RUNX2 expression in human VICs.

A, Diagram of proximity ligation assay (PLA, left panel). Representative images of TERT/STAT5 complex (red foci) in CAVD VICs cultured for 21 days in osteogenic medium and detected by PLA. Scalebar 100 µm (middle panel). Quantification of PLA signal is shown in the right graph. n = 4. B, Logo analysis depicting the consensus binding site for tetrameric STAT5 (top panel). Diagram depicting STAT5 and TERT binding RUNX2 promoter and the positions of the predictedSTAT5 binding sites (bottom panel). C, STAT5 (left graphs) and TERT (right graphs) enrichment on the RUNX2 promoter of control VICs after 14 days of osteogenic stimulation and quantified by ChIP-qPCR. n = 4. D, Representative images of control and CAVD VICs treated with 10 µM of the STAT5 inhibitors StafiA-1or StafiB-1 during 28 days of osteogenic stimulation. Scalebar 400 µm. n = 8, means ± SD. Quantification of calcification is shown on the right graph. Data are shown as means ± SD. *P* values were calculated by the Mann-Whitney *U* test (Figure A and C) and Kruskal-Wallis *H* test (Figure D) and indicated on each graph.

Figure 7. TERT and STAT5 are upregulated and colocalize in CAVD tissue.

A, Representative serial sections of Von Kossa (dark precipitation, top panels) and TERT and STAT5 immunofluorescent staining (bottom panels) in control and CAVD valve tissues. Scalebar100 µm. Quantification of STAT5 intensity and STAT5-positive cells (STAT5+) are shown on the right panels. B, Quantification of STAT5-TERT-positive cells. Data are shown as means ± SD, n = 5 control, n = 6 CAVD. *P* values were calculated with the Mann-Whitney *U* test and indicated on each graph.

Figure 8. TERT/STAT5 promotes osteogenic reprogramming

Inflammation promotes the upregulation and interaction of TERT and STAT5. Then, the TERT/STAT5 complex translocates into the nucleus where TERT facilitates STAT5 binding to

630 the promoter region of *RUNX2* gene, to engage the osteogenic reprogramming of VICs during
631 the early stages of CAVD pathogenesis.

632

633 **Supplemental Figure 1. Characterization of human CAVD valves and correlation of TERT**
634 **expression with age.** A, Representative section of Von Kossa staining in control and valve
635 CAVD leaflets tissue. Scalebar 1 mm. B, Representative serial sections of RUNX2
636 immunofluorescent staining (top panels) and OPN (bottom panels) in control and CAVD valve
637 tissues. Scalebar 100 µm. Quantification of RUNX2-positive cells and OPN-positive cells on the
638 leaflet specimen is shown on the right graphs. n = 5 control, n = 6 CAVD. C, Correlation
639 between age of the donor and *TERT* expression. n = 8 control, n = 9 CAVD, Pearson correlation
640 test. D, Expression profile in the subject leaflets. n = 7 control, n = 7 CAVD. E, Confocal images
641 of a CAVD leaflet. Scalebar 50 µm. F, Representative images of immunofluorescent staining of
642 PCNA (top panels) and γ-H2AX (bottom panels) in control and CAVD valve tissues. Scalebar
643 100 µm. Quantification of PCNA-positive cells and γ-H2AX-positive cells are shown on the right
644 graphs. n = 4 control, n = 3 CAVD. Data are shown as means ± SD. *P* values were calculated
645 with the Mann-Whitney *U* test (Figures B, G, and F) and two-way ANOVA with the Sidak post
646 hoc test (heatmap on D).

647

648 **Supplemental Figure 2. VIC migration, activation, and osteogenic markers at baseline.**
649 A, Representative images of a scratch assay in control (top panels) and CAVD (bottom panels)
650 VICs. Time points are indicated on top of each panel. Blue lines denote the cell migration front.
651 Scalebar 1 mm. n = 10 control, n = 10 CAVD. B, Representative images of αSMA and CNN (top
652 panels) and SM22 (bottom panels) in control and CAVD VICs. Scalebar 50 µm. Signal

quantification of αSMA, CNN, and SM22 are shown on the right panels. n = 4 control, n = 4 CAVD. C, Representative images of TNAP and f-Actin signal in control and CAVD VICs. Scalebar 50 µm. Signal quantification of TNAP and f-Actin is shown on the right panels. n = 4 control, n = 4 CAVD. Data are shown as means ± SD. *P* values were calculated with the Mann-Whitney *U* test and shown on top of each graph.

Supplemental Figure 3. Senescence is not operative during the osteogenic differentiation of VICs.

A, Cell counting of control and CAVD VICs after 14 days of NT or OST stimulation. n = 4 control, n = 4 CAVD. B, β-galactosidase (*BGLAP*) mRNA transcript quantification in control and CAVD VICs at baseline. n = 5 control, n= 4 CAVD. C, Representative images of senescence-associated β-galactosidase activity staining of VICs after 28 days of NT or OST stimulation. Blue cells were considered positive for senescence. Quantification of senescence is shown on the right graph. n = 4 control; n = 4 CAVD. Data are shown as means ± SD. *P* values were calculated with the Mann-Whitney *U* test (figure A and B) and the Kruskal-Wallis *H* test with Dunn post hoc test and shown on top of each graph.

Supplemental Figure 4. TERT is upregulated and required for the osteogenic differentiation of human mesenchymal stem cells.

A, Representative images of human MSCs stimulated with OST for 14 days. Calcium deposition was visualized by Alizarin Red staining. Quantification of calcification is shown on the right graph. n = 3. Scalebar 50 µm. B, Western blot staining of samples from MSCs collected during the 14 days of OST treatment. C, TERT and RUNX2 expression profile of differentiating MSCs stimulated for 14 days with OST media. n = 3. D, Representative TERT immunofluorescent staining images of MSCs stimulated with osteogenic media for 14 days. Scalebar 100 µm. E,

MSCs transduced with lentivirus containing either shControl-GFP or shTERT-GFP and stimulated with osteogenic media for up to 21 days. Quantification of calcification is shown on the right graph. n = 4; means ± SD. F, Representative western blot staining of MSCs transduced with lentivirus containing either shControl-GFP or shTERT-GFP followed by 7 days of osteogenic stimulation. Data are shown as means ± SD. *P* values were calculated by Kruskal-Wallis *H* test with Dunn pairwise comparison post hoc test (Figure C) and two-way ANOVA with Tukey post hoc test (Figures A and E).

Supplemental Figure 5. Senescence is not operative in mice Tert -/- cells.

A, Representative images of a senescence-associated β-galactosidase (SA-β-gal) staining of mVICs isolated from wild-type (*Tert* $^{+/+}$) or F1 Tert knockout (*Tert* $^{-/-}$) mice after 21 days of OST stimulation. Blue cells were considered positive for senescence. Quantification of senescence cells is shown on the right graph. B, Representative images of SA-β-gal staining of mBMMSCs isolated from *Tert* $^{+/+}$ or *Tert* $^{-/-}$ mice after 21 days of osteogenic stimulation. Blue cells were considered positive for senescence. Quantification of senescence is shown on the right graph. Both figures, n = 5 *Tert* $^{+/+}$, n = 3 *Tert* -/-. Scalebar 400 μm. Data are shown as means ± SD. *P* values were calculated with the Mann-Whitney *U* test and shown on each graph.

Supplemental Data Fig 6. STAT5 is upregulated and required during osteogenic differentiation of VICs.

A, Representative western blot staining of samples from CAVD and control VICs after 14 days of OST stimulation. Quantification of protein levels is shown on the right graphs. n = 4, control n = 4 CAVD. B, Representative immunofluorescence image of STAT5 shows subcellular distribution after 14 days of NT and OST stimulation. Scalebar 40 μm. C, Representative images of TERT/STAT5 complex (red foci) in control VICs and detected by proximity ligation assay (PLA).

Scalebar 100 µm. Quantification of PLA is shown on the right graph. n = 4. D, Representative images of CASMCs (left panels) treated with 10 µM of the STAT5 inhibitors StafiA-1 or StafiB-1 during the 14 days of OST stimulation. Scalebar 400 µm. Quantification of calcification is shown on the right graph. n = 4.E, Representative images of MSCs (left panels) treated with 10 µM of the STAT5 inhibitors StafiA-1 or StafiB-1 during the 21 days of OST stimulation. Scalebar 400 µm. Quantification of calcification is shown on the right graph. n = 4. F, Representative immunofluorescence images of VICs after 14 days of LPS treatment or OST stimulation. Scalebar 50 µm. G, Representative western blot staining of CAVD VICs after 14 days of OST stimulation. Data are shown as means ± SD. *P* values were calculated with the Mann-Whitney *U* test (Figures A and B) and the Kruskal-Wallis *H* test with Dunn pairwise comparison post-test (Figured D and E) and indicated in each graph.

REFERENCES

1. Kraler S, Blaser MC, Aikawa E, Camici GG, Luscher TF. Calcific aortic valve disease: from molecular and cellular mechanisms to medical therapy. *Eur Heart J*. 2022;43:683-697. doi: 10.1093/eurheartj/ehab757
2. Buttner P, Feistner L, Lurz P, Thiele H, Hutcheson JD, Schlotter F. Dissecting Calcific Aortic Valve Disease-The Role, Etiology, and Drivers of Valvular Fibrosis. *Front Cardiovasc Med*. 2021;8:660797. doi: 10.3389/fcvm.2021.660797
3. Coffey S, Roberts-Thomson R, Brown A, Carapetis J, Chen M, Enriquez-Sarano M, Zuhlke L, Prendergast BD. Global epidemiology of valvular heart disease. *Nat Rev Cardiol*. 2021;18:853-864. doi: 10.1038/s41569-021-00570-z
4. Roth GA, Mensah GA, Johnson CO, Addolorato G, Ammirati E, Baddour LM, Barengo NC, Beaton AZ, Benjamin EJ, Benziger CP, et al. Global Burden of Cardiovascular Diseases and Risk Factors, 1990-2019: Update From the GBD 2019 Study. *J Am Coll Cardiol*. 2020;76:2982-3021. doi: 10.1016/j.jacc.2020.11.010
5. Yutzey KE, Demer LL, Body SC, Huggins GS, Towler DA, Giachelli CM, Hofmann-Bowman MA, Mortlock DP, Rogers MB, Sadeghi MM, et al. Calcific aortic valve disease:

a consensus summary from the Alliance of Investigators on Calcific Aortic Valve Disease. *Arterioscler Thromb Vasc Biol*. 2014;34:2387-2393. doi: 10.1161/ATVBAHA.114.302523

6. Virani SS, Alonso A, Benjamin EJ, Bittencourt MS, Callaway CW, Carson AP, Chamberlain AM, Chang AR, Cheng S, Delling FN, et al. Heart Disease and Stroke Statistics-2020 Update: A Report From the American Heart Association. *Circulation*. 2020;141:e139-e596. doi: 10.1161/CIR.0000000000000757

7. Rajamannan NM, Evans FJ, Aikawa E, Grande-Allen KJ, Demer LL, Heistad DD, Simmons CA, Masters KS, Mathieu P, O'Brien KD, et al. Calcific aortic valve disease: not simply a degenerative process: A review and agenda for research from the National Heart and Lung and Blood Institute Aortic Stenosis Working Group. Executive summary: Calcific aortic valve disease-2011 update. *Circulation*. 2011;124:1783-1791. doi: 10.1161/CIRCULATIONAHA.110.006767

8. Chen JH, Simmons CA. Cell-matrix interactions in the pathobiology of calcific aortic valve disease: critical roles for matricellular, matricrine, and matrix mechanics cues. *Circ Res*. 2011;108:1510-1524. doi: 10.1161/CIRCRESAHA.110.234237

9. Liu AC, Joag VR, Gotlieb AI. The emerging role of valve interstitial cell phenotypes in regulating heart valve pathobiology. *Am J Pathol*. 2007;171:1407-1418. doi: 10.2353/ajpath.2007.070251

10. Rajamannan NM, Subramaniam M, Rickard D, Stock SR, Donovan J, Springett M, Orszulak T, Fullerton DA, Tajik AJ, Bonow RO, et al. Human aortic valve calcification is associated with an osteoblast phenotype. *Circulation*. 2003;107:2181-2184. doi: 10.1161/01.CIR.0000070591.21548.69

11. Rajamannan NM. Calcific aortic valve disease: cellular origins of valve calcification. *Arterioscler Thromb Vasc Biol*. 2011;31:2777-2778. doi: 10.1161/ATVBAHA.111.237610

12. Aikawa E, Libby P. A Rock and a Hard Place: Chiseling Away at the Multiple Mechanisms of Aortic Stenosis. *Circulation*. 2017;135:1951-1955. doi: 10.1161/CIRCULATIONAHA.117.027776

13. Wirrig EE, Yutzey KE. Conserved transcriptional regulatory mechanisms in aortic valve development and disease. *Arterioscler Thromb Vasc Biol*. 2014;34:737-741. doi: 10.1161/ATVBAHA.113.302071

14. Calado RT, Young NS. Telomere diseases. *N Engl J Med*. 2009;361:2353-2365. doi: 10.1056/NEJMra0903373

15. Stewart SA, Hahn WC, O'Connor BF, Banner EN, Lundberg AS, Modha P, Mizuno H, Brooks MW, Fleming M, Zimonjic DB, et al. Telomerase contributes to tumorigenesis by a telomere length-independent mechanism. *Proc Natl Acad Sci U S A*. 2002;99:12606-12611. doi: 10.1073/pnas.182407599

16. Choi J, Southworth LK, Sarin KY, Venteicher AS, Ma W, Chang W, Cheung P, Jun S, Artandi MK, Shah N, et al. TERT promotes epithelial proliferation through transcriptional control of a Myc- and Wnt-related developmental program. *PLoS Genet*. 2008;4:e10. doi: 10.1371/journal.pgen.0040010

17. Masutomi K, Possemato R, Wong JM, Currier JL, Tothova Z, Manola JB, Ganesan S, Lansdorp PM, Collins K, Hahn WC. The telomerase reverse transcriptase regulates chromatin state and DNA damage responses. *Proc Natl Acad Sci U S A*. 2005;102:8222-8227. doi: 10.1073/pnas.0503095102

18. Park JI, Venteicher AS, Hong JY, Choi J, Jun S, Shkreli M, Chang W, Meng Z, Cheung P, Ji H, et al. Telomerase modulates Wnt signalling by association with target gene chromatin. *Nature*. 2009;460:66-72. doi: 10.1038/nature08137

19. Aono J, Ruiz-Rodriguez E, Qing H, Findeisen HM, Jones KL, Heywood EB, Bruemmer D. Telomerase Inhibition by Everolimus Suppresses Smooth Muscle Cell Proliferation and Neointima Formation Through Epigenetic Gene Silencing. *JACC Basic Transl Sci*. 2016;1:49-60. doi: 10.1016/j.jacbts.2016.01.002

20. Endorf EB, Qing H, Aono J, Terami N, Doyon G, Hyzny E, Jones KL, Findeisen HM, Bruemmer D. Telomerase Reverse Transcriptase Deficiency Prevents Neointima Formation Through Chromatin Silencing of E2F1 Target Genes. *Arterioscler Thromb Vasc Biol*. 2017;37:301-311. doi: 10.1161/ATVBAHA.116.308717

21. Shi S, Gronthos S, Chen S, Reddi A, Counter CM, Robey PG, Wang CY. Bone formation by human postnatal bone marrow stromal stem cells is enhanced by telomerase expression. *Nat Biotechnol*. 2002;20:587-591. doi: 10.1038/nbt0602-587

22. Simonsen JL, Rosada C, Serakinci N, Justesen J, Stenderup K, Rattan SI, Jensen TG, Kassem M. Telomerase expression extends the proliferative life-span and maintains the osteogenic potential of human bone marrow stromal cells. *Nat Biotechnol*. 2002;20:592-596. doi: 10.1038/nbt0602-592

23. Cuevas RA, Chu CC, Moorhead WJ, 3rd, Wong R, Sultan I, St Hilaire C. Isolation of Human Primary Valve Cells for In vitro Disease Modeling. *J Vis Exp*. 2021:e62439. doi: 10.3791/62439

24. Ducy P, Zhang R, Geoffroy V, Ridall AL, Karsenty G. Osf2/Cbfa1: a transcriptional activator of osteoblast differentiation. *Cell*. 1997;89:747-754. doi: 10.1016/s0092-8674(00)80257-3

25. Sun Y, Byon CH, Yuan K, Chen J, Mao X, Heath JM, Javed A, Zhang K, Anderson PG, Chen Y. Smooth muscle cell-specific runx2 deficiency inhibits vascular calcification. *Circ Res*. 2012;111:543-552. doi: 10.1161/CIRCRESAHA.112.267237

26. Parra-Izquierdo I, Castanos-Mollor I, Lopez J, Gomez C, San Roman JA, Sanchez Crespo M, Garcia-Rodriguez C. Calcification Induced by Type I Interferon in Human Aortic Valve Interstitial Cells Is Larger in Males and Blunted by a Janus Kinase Inhibitor. *Arterioscler Thromb Vasc Biol*. 2018;38:2148-2159. doi: 10.1161/ATVBAHA.118.311504

27. Parra-Izquierdo I, Castanos-Mollor I, Lopez J, Gomez C, San Roman JA, Sanchez Crespo M, Garcia-Rodriguez C. Lipopolysaccharide and interferon-gamma team up to activate HIF-1alpha via STAT1 in normoxia and exhibit sex differences in human aortic valve interstitial cells. *Biochim Biophys Acta Mol Basis Dis*. 2019;1865:2168-2179. doi: 10.1016/j.bbadis.2019.04.014

28. Jin H, St Hilaire C, Huang Y, Yang D, Dmitrieva NI, Negro A, Schwartzbeck R, Liu Y, Yu Z, Walts A, et al. Increased activity of TNAP compensates for reduced adenosine production and promotes ectopic calcification in the genetic disease ACDC. *Sci Signal*. 2016;9:ra121. doi: 10.1126/scisignal.aaf9109

29. Moorhead WJ, 3rd, Chu CC, Cuevas RA, Callahan Jt, Wong R, Regan C, Boufford CK, Sur S, Liu M, Gomez D, et al. Dysregulation of FOXO1 (Forkhead Box O1 Protein) Drives Calcification in Arterial Calcification due to Deficiency of CD73 and Is Present in Peripheral Artery Disease. *Arterioscler Thromb Vasc Biol*. 2020;40:1680-1694. doi: 10.1161/ATVBAHA.119.313765

30. Jung JJ, Razavian M, Kim HY, Ye Y, Golestani R, Toczek J, Zhang J, Sadeghi MM. Matrix metalloproteinase inhibitor, doxycycline and progression of calcific aortic valve disease in hyperlipidemic mice. *Sci Rep*. 2016;6:32659. doi: 10.1038/srep32659

31. Millan A, Lanzer P, Sorribas V. The Thermodynamics of Medial Vascular Calcification. *Front Cell Dev Biol*. 2021;9:633465. doi: 10.3389/fcell.2021.633465

32. Kim NW, Piatyszek MA, Prowse KR, Harley CB, West MD, Ho PL, Coviello GM, Wright WE, Weinrich SL, Shay JW. Specific association of human telomerase activity with immortal cells and cancer. *Science*. 1994;266:2011-2015. doi: 10.1126/science.7605428

33. Hao LY, Armanios M, Strong MA, Karim B, Feldser DM, Huso D, Greider CW. Short telomeres, even in the presence of telomerase, limit tissue renewal capacity. *Cell*. 2005;123:1121-1131. doi: 10.1016/j.cell.2005.11.020

34. Pascolo E, Wenz C, Lingner J, Hauel N, Priepke H, Kauffmann I, Garin-Chesa P, Rettig WJ, Damm K, Schnapp A. Mechanism of human telomerase inhibition by BIBR1532, a synthetic, non-nucleosidic drug candidate. *J Biol Chem*. 2002;277:15566-15572. doi: 10.1074/jbc.M201266200

35. Ogawa D, Nomiyama T, Nakamachi T, Heywood EB, Stone JF, Berger JP, Law RE, Bruemmer D. Activation of peroxisome proliferator-activated receptor gamma suppresses telomerase activity in vascular smooth muscle cells. *Circ Res*. 2006;98:e50-59. doi: 10.1161/01.RES.0000218271.93076.c3

36. Chiang YJ, Hemann MT, Hathcock KS, Tessarollo L, Feigenbaum L, Hahn WC, Hodes RJ. Expression of telomerase RNA template, but not telomerase reverse transcriptase, is limiting for telomere length maintenance in vivo. *Mol Cell Biol*. 2004;24:7024-7031. doi: 10.1128/MCB.24.16.7024-7031.2004

37. Ghosh A, Saginc G, Leow SC, Khattar E, Shin EM, Yan TD, Wong M, Zhang Z, Li G, Sung WK, et al. Telomerase directly regulates NF-kappaB-dependent transcription. *Nat Cell Biol*. 2012;14:1270-1281. doi: 10.1038/ncb2621

38. Liu N, Ding D, Hao W, Yang F, Wu X, Wang M, Xu X, Ju Z, Liu JP, Song Z, et al. hTERT promotes tumor angiogenesis by activating VEGF via interactions with the Sp1 transcription factor. *Nucleic Acids Res*. 2016;44:8693-8703. doi: 10.1093/nar/gkw549

39. Lee C, Huang CH. LASAGNA: a novel algorithm for transcription factor binding site alignment. *BMC Bioinformatics*. 2013;14:108. doi: 10.1186/1471-2105-14-108

40. Wingender E, Dietze P, Karas H, Knuppel R. TRANSFAC: a database on transcription factors and their DNA binding sites. *Nucleic Acids Res*. 1996;24:238-241. doi: 10.1093/nar/24.1.238

41. Okutani Y, Kitanaka A, Tanaka T, Kamano H, Ohnishi H, Kubota Y, Ishida T, Takahara J. Src directly tyrosine-phosphorylates STAT5 on its activation site and is involved in erythropoietin-induced signaling pathway. *Oncogene*. 2001;20:6643-6650. doi: 10.1038/sj.onc.1204807

42. Natarajan K, Muller-Klieser D, Rubner S, Berg T. Stafia-1: a STAT5a-Selective Inhibitor Developed via Docking-Based Screening of in Silico O-Phosphorylated Fragments. *Chemistry*. 2020;26:148-154. doi: 10.1002/chem.201904147

43. Elumalai N, Berg A, Natarajan K, Scharow A, Berg T. Nanomolar inhibitors of the transcription factor STAT5b with high selectivity over STAT5a. *Angew Chem Int Ed Engl*. 2015;54:4758-4763. doi: 10.1002/anie.201410672

44. Leopold JA. Cellular mechanisms of aortic valve calcification. *Circ Cardiovasc Interv*. 2012;5:605-614. doi: 10.1161/CIRCINTERVENTIONS.112.971028

45. Babu AN, Meng X, Zou N, Yang X, Wang M, Song Y, Cleveland JC, Weyant M, Banerjee A, Fullerton DA. Lipopolysaccharide stimulation of human aortic valve interstitial cells activates inflammation and osteogenesis. *Ann Thorac Surg*. 2008;86:71-76. doi: 10.1016/j.athoracsur.2008.03.008

46. Gizard F, Nomiyama T, Zhao Y, Findeisen HM, Heywood EB, Jones KL, Staels B, Bruemmer D. The PPARalpha/p16INK4a pathway inhibits vascular smooth muscle cell proliferation by repressing cell cycle-dependent telomerase activation. *Circ Res*. 2008;103:1155-1163. doi: 10.1161/CIRCRESAHA.108.186205

47. Maida Y, Yasukawa M, Okamoto N, Ohka S, Kinoshita K, Totoki Y, Ito TK, Minamino T, Nakamura H, Yamaguchi S, et al. Involvement of telomerase reverse transcriptase in heterochromatin maintenance. *Mol Cell Biol*. 2014;34:1576-1593. doi: 10.1128/MCB.00093-14

48. Okamoto N, Yasukawa M, Nguyen C, Kasim V, Maida Y, Possemato R, Shibata T, Ligon KL, Fukami K, Hahn WC, et al. Maintenance of tumor initiating cells of defined genetic composition by nucleostemin. *Proc Natl Acad Sci U S A*. 2011;108:20388-20393. doi: 10.1073/pnas.1015171108

49. Slagboom PE, Droog S, Boomsma DI. Genetic determination of telomere size in humans: a twin study of three age groups. *Am J Hum Genet*. 1994;55:876-882.

50. Brouilette S, Singh RK, Thompson JR, Goodall AH, Samani NJ. White cell telomere length and risk of premature myocardial infarction. *Arterioscler Thromb Vasc Biol*. 2003;23:842-846. doi: 10.1161/01.ATV.0000067426.96344.32

51. Samani NJ, Boultby R, Butler R, Thompson JR, Goodall AH. Telomere shortening in atherosclerosis. *Lancet*. 2001;358:472-473. doi: 10.1016/S0140-6736(01)05633-1

52. Kurz DJ, Kloeckener-Gruissem B, Akhmedov A, Eberli FR, Buhler I, Berger W, Bertel O, Luscher TF. Degenerative aortic valve stenosis, but not coronary disease, is associated with shorter telomere length in the elderly. *Arterioscler Thromb Vasc Biol*. 2006;26:e114-117. doi: 10.1161/01.ATV.0000222961.24912.69

53. Huzen J, Peeters W, de Boer RA, Moll FL, Wong LS, Codd V, de Kleijn DP, de Smet BJ, van Veldhuisen DJ, Samani NJ, et al. Circulating leukocyte and carotid atherosclerotic plaque telomere length: interrelation, association with plaque characteristics, and restenosis after endarterectomy. *Arterioscler Thromb Vasc Biol*. 2011;31:1219-1225. doi: 10.1161/ATVBAHA.110.217158

54. Hoerstrup SP, Kadner A, Melnitchouk S, Trojan A, Eid K, Tracy J, Sodian R, Visjager JF, Kolb SA, Grunenfelder J, et al. Tissue engineering of functional trileaflet heart valves from human marrow stromal cells. *Circulation*. 2002;106:I143-150.

55. Hortells L, Sur S, St Hilaire C. Cell Phenotype Transitions in Cardiovascular Calcification. *Front Cardiovasc Med*. 2018;5:27. doi: 10.3389/fcvm.2018.00027

56. Bogdanova M, Zabirnyk A, Malashicheva A, Enayati KZ, Karlsen TA, Kaljusto ML, Kvitting JP, Dissen E, Sullivan GJ, Kostareva A, et al. Interstitial cells in calcified aortic valves have reduced differentiation potential and stem cell-like properties. *Sci Rep*. 2019;9:12934. doi: 10.1038/s41598-019-49016-0

57. Lin ME, Chen T, Leaf EM, Speer MY, Giachelli CM. Runx2 Expression in Smooth Muscle Cells Is Required for Arterial Medial Calcification in Mice. *Am J Pathol*. 2015;185:1958-1969. doi: 10.1016/j.ajpath.2015.03.020

58. Xu K, Xie S, Huang Y, Zhou T, Liu M, Zhu P, Wang C, Shi J, Li F, Sellke FW, et al. Cell-Type Transcriptome Atlas of Human Aortic Valves Reveal Cell Heterogeneity and Endothelial to Mesenchymal Transition Involved in Calcific Aortic Valve Disease. *Arterioscler Thromb Vasc Biol*. 2020;40:2910-2921. doi: 10.1161/ATVBAHA.120.314789

59. Joung YH, Lim EJ, Darvin P, Chung SC, Jang JW, Do Park K, Lee HK, Kim HS, Park T, Yang YM. MSM enhances GH signaling via the Jak2/STAT5b pathway in osteoblast-like cells and osteoblast differentiation through the activation of STAT5b in MSCs. *PLoS One*. 2012;7:e47477. doi: 10.1371/journal.pone.0047477

60. Lee KM, Park KH, Hwang JS, Lee M, Yoon DS, Ryu HA, Jung HS, Park KW, Kim J, Park SW, et al. Inhibition of STAT5A promotes osteogenesis by DLX5 regulation. *Cell Death Dis*. 2018;9:1136. doi: 10.1038/s41419-018-1184-7

61. Paulson M, Pisharody S, Pan L, Guadagno S, Mui AL, Levy DE. Stat protein transactivation domains recruit p300/CBP through widely divergent sequences. *J Biol Chem*. 1999;274:25343-25349. doi: 10.1074/jbc.274.36.25343

62. Martino A, Holmes JHt, Lord JD, Moon JJ, Nelson BH. Stat5 and Sp1 regulate transcription of the cyclin D2 gene in response to IL-2. *J Immunol*. 2001;166:1723-1729. doi: 10.4049/jimmunol.166.3.1723

63. Bergad PL, Towle HC, Berry SA. Yin-yang 1 and glucocorticoid receptor participate in the Stat5-mediated growth hormone response of the serine protease inhibitor 2.1 gene. *J Biol Chem*. 2000;275:8114-8120. doi: 10.1074/jbc.275.11.8114

64. Yamada O, Ozaki K, Furukawa T, Machida M, Wang YH, Motoji T, Mitsuishi T, Akiyama M, Yamada H, Kawauchi K, et al. Activation of STAT5 confers imatinib resistance on leukemic cells through the transcription of TERT and MDR1. *Cell Signal*. 2011;23:1119-1127. doi: 10.1016/j.cellsig.2011.02.005

65. Yamada O, Ozaki K, Akiyama M, Kawauchi K. JAK-STAT and JAK-PI3K-mTORC1 pathways regulate telomerase transcriptionally and posttranslationally in ATL cells. *Mol Cancer Ther*. 2012;11:1112-1121. doi: 10.1158/1535-7163.MCT-11-0850

66. Tormo AJ, Letellier MC, Sharma M, Elson G, Crabe S, Gauchat JF. IL-6 activates STAT5 in T cells. *Cytokine*. 2012;60:575-582. doi: 10.1016/j.cyto.2012.07.002

67. Tanabe Y, Nishibori T, Su L, Arduini RM, Baker DP, David M. Cutting edge: role of STAT1, STAT3, and STAT5 in IFN-alpha beta responses in T lymphocytes. *J Immunol*. 2005;174:609-613. doi: 10.4049/jimmunol.174.2.609

68. Honda S, Miyamoto T, Watanabe T, Narumi T, Kadowaki S, Honda Y, Otaki Y, Hasegawa H, Netsu S, Funayama A, et al. A novel mouse model of aortic valve stenosis induced by direct wire injury. *Arterioscler Thromb Vasc Biol*. 2014;34:270-278. doi: 10.1161/ATVBAHA.113.302610

69. Sider KL, Blaser MC, Simmons CA. Animal models of calcific aortic valve disease. *Int J Inflam*. 2011;2011:364310. doi: 10.4061/2011/364310

70. Balani K, Brito FC, Kos L, Agarwal A. Melanocyte pigmentation stiffens murine cardiac tricuspid valve leaflet. *J R Soc Interface*. 2009;6:1097-1102. doi: 10.1098/rsif.2009.0174

71. Carneiro F, Kruithof BP, Balani K, Agarwal A, Gaussin V, Kos L. Relationships between melanocytes, mechanical properties and extracellular matrix composition in mouse heart valves. *J Long Term Eff Med Implants*. 2015;25:17-26. doi: 10.1615/jlongtermeffmedimplants.2015011748

72. Mjaatvedt CH, Kern CB, Norris RA, Fairey S, Cave CL. Normal distribution of melanocytes in the mouse heart. *Anat Rec A Discov Mol Cell Evol Biol*. 2005;285:748-757. doi: 10.1002/ar.a.20210

958 73. Dharmarajan S, Speer MY, Pierce K, Lally J, Leaf EM, Lin ME, Scatena M, Giachelli CM.
959 Role of Runx2 in Calcific Aortic Valve Disease in Mouse Models. *Front Cardiovasc Med*.
960 2021;8:687210. doi: 10.3389/fcvm.2021.687210
961

SUPPLEMENTAL MATERIAL

Non-canonical Telomerase Reverse Transcriptase Controls Osteogenic Differentiation of Aortic Valve Cells Through STAT5

Rolando A. Cuevas[1], Luis Hortells[1,2], Claire C. Chu[1], Ryan Wong[1], Alex Crane[1], Camille Boufford[1], Cailyn Regan[1], William J. Moorhead III[1], Michael J. Bashline[1], Aneesha Parwal[1], Angelina M. Parise[1], Aditi Gurkar[3], Dennis Bruemmer[4], John Sembrat[5], Ibrahim Sultan[6], Thomas G. Gleason[7], Marie Billaud[8], and Cynthia St. Hilaire[1,9*]

[1] Division of Cardiology, Department of Medicine, Pittsburgh Heart, Lung, Blood and Vascular Medicine Institute, University of Pittsburgh, Pittsburgh, Pennsylvania, USA.

[2] current address - Institute for Experimental Cardiovascular Medicine, University Heart Centre Freiburg–Bad Krozingen, Medical Center and Faculty of Medicine, University of Freiburg, Freiburg, Germany.

[3] Aging Institute, Division of Geriatrics, Department of Medicine, University of Pittsburgh, Pittsburgh, Pennsylvania, USA.

[4] Department of Cardiovascular Medicine, Cleveland Clinic, Cleveland, OH, USA.

[5] Division of Pulmonary, Allergy, and Critical Care Medicine, University of Pittsburgh School of Medicine, Pittsburgh, PA, USA.

[6] Division of Cardiac Surgery, Department of Cardiothoracic Surgery, Heart and Vascular Institute, University of Pittsburgh Medical Center, Pittsburgh, Pennsylvania, USA.

[7] Division of Cardiac Surgery, Univ. of Maryland School of Medicine, Baltimore, MD, USA.

[8] Department of Surgery, Division of Cardiac Surgery, Brigham and Women's Hospital & Harvard Medical School, Boston, Maryland, USA.

[9] Department of Bioengineering, University of Pittsburgh, Pittsburgh, Pennsylvania, USA.

Running Title: TERT/STAT5 is required for cardiovascular calcification

*Corresponding Author Contact Info:
Cynthia St. Hilaire, PhD, FAHA
University of Pittsburgh
BSTWR 1744.1
200 Lothrop Street, Pittsburgh, PA 15261
+1 412-648-9441 sthilair@pitt.edu

*Corresponding Author Contact Info:
Cynthia St. Hilaire, PhD, FAHA
University of Pittsburgh
BSTWR 1744.1
200 Lothrop Street, Pittsburgh, PA 15261
+1 412-648-9441 sthilair@pitt.edu

METHODS

Availability of Materials

We abide by the NIH Grants Policy on Sharing of Unique Research Resources, including the NIH Policy on Sharing of Model Organisms for Biomedical Research (2004), NIH Grants Policy Statement (2003), and Sharing of Biomedical Research Resources: Principles and Guidelines for Recipients of NIH Grants and Contracts (1999), and the Bayh-Dole Act and the Technology Transfer Commercialization Act of 2000. De-identified human cell lines and tissues generated in our laboratory will be made available for non-commercial research per established University of Pittsburgh Office of Research IRB and MTA protocols.

Ethics

Human aortic valves were collected from subjects enrolled in studies approved by the institutional review board (IRB) of the University of Pittsburgh per the Declaration of Helsinki. No bicuspid valves were used in this study. Mice used for the generation of cell lines were given veterinary care by the University of Pittsburgh Division of Laboratory Animal Resources which adheres to the NIH policy on the Animal Welfare Act and all other applicable laws. Facilities are under the full-time supervision of veterinarians and are AAALAC-accredited. Our protocols follow the AVMA Guidelines on Euthanasia. All animal use was approved by the Institutional Animal Care and Use Committee at the University of Pittsburgh.

Human Tissue Collection and Isolation

Surgical specimens from humans were collected from subjects who consented and enrolled in studies approved by the institutional review board (IRB) of the University of Pittsburgh per the

Declaration of Helsinki. Personnel involved with specimen handling underwent extensive institutional training. Cadaveric tissues obtained via the Center for Organ Recovery and Education (CORE) were approved by the University of Pittsburgh Committee for Oversight of Research and Clinical Training Involving Decedents (CORID). A detailed protocol describing tissue collection handling was published previously.[1] Briefly, valves were collected from valve replacement surgeries or recovered from cadaveric organs and stored in cold Belzer UW Cold Storage Transplant Solution (Bridge to Life) at 4°C for transporting. Aortic roots were excised and washed with a sterile rinsing solution (sterile PBS supplemented with 2.5 µg/mL of fungicide, 0.05 mg/mL of gentamicin, and 5 µg/mL of bactericide). Leaflets were unbiasedly selected for VIC isolation, Von Kossa staining for calcification, and snap freezing for RNA collection. Tissues were processed as close as possible to the time of extraction to guarantee the best yield of cell recovery.

Human Cell Isolation

We established patient-specific lines by using the same valves for histopathology, RNA, and cell isolation. Human primary aortic valve interstitial cell (VIC) lines were generated from male and female subjects as previously described.[2] Briefly, leaflets were washed with PBS containing 10 mg/ml gentamicin (GIBCO) and 250 µg/ml fungizone (GIBCO) and dissociated with 0.1% collagenase II at 37 C and 5% of CO2 for 18 hours. Then, the tissue was further dissociated by gently mixing it by pipetting with a serological pipette to ensure the release of AVICs and then passed through a 0.70 µm filter to remove debris. Cells were pelleted and then resuspended in Dulbecco's Modified Eagle's Medium (DMEM) supplemented with 10% fetal bovine serum (FBS) and 1X penicillin-streptomycin (P/S). Human coronary artery smooth muscle cells (CASMC) were obtained from the patient coronary as previously described.[3] Briefly, vessels were washed

with PBS containing 10 mg/ml gentamicin (GIBCO) and 250 µg/ml fungizone (GIBCO). Vessels were cut open to expose the lumen and intima and adventitia were gently scrapped. Vessels were then sectioned and dissociated with 0.1% collagenase II for 3 hrs. Cells were pelleted and then seeded and expanded.

Cell Culture

VIC lines were expanded in Dulbecco's Modified Eagle's Medium supplemented with 10% fetal bovine serum and 1X penicillin-streptomycin. Cells were used between passages 4 and 15. Growth media was changed every three days, and cells were split 1:2 when confluent. Human coronary artery smooth muscle cell (CASMC) lines were expanded in smooth muscle media SMGM (CC-3181) supplemented with BULLETKIT (CC-4149). Human mesenchymal stem cells (MSCs, PT-2501, Lonza) were expanded on Minimum Essential Medium alpha without nucleosides and supplemented with 10% fetal bovine serum and 1X penicillin-streptomycin and used between passages 4 and 10. Cells are routinely tested for mycoplasma contamination.

Osteogenic Assay

For osteogenic experiments, 250,000 cells per 9.5 cm^2 were seeded and treated with osteogenic media (Gibco Minimum Essential Medium alpha with nucleosides, 10% FBS, 1X P/S, 10 mM glycerol phosphate, 50 µM ascorbic acid 2-phosphate, and 100 nM dexamethasone).[4] No treatment media consisted of Gibco Minimum Essential Medium alpha with nucleosides, 10% FBS, 1X P/S. Media was replaced every four days and prepared fresh every time. BiBR1532 (2981, Tocris) was added to the media at 1, 10, or 100 nM every two days during the OST treatment.[5] Inhibitors StafiA-1 and StafiB-1 (Sigma-Aldrich) were used at 10 µM and added every two days for the duration of the OST treatment. For inflammatory

assays, we used 2.5 µg/mL of LPS from Escherichia coli O111:B4 (Sigma-Aldrich) every two days for the duration of the OST treatment.

SDS-Page and Immunoblotting

Cells were lysed in lysis buffer (1% CHAPS hydrate, 150 mM sodium chloride, 25 mM HEPES buffer), supplemented with 1x protease and phosphatase inhibitor cocktail (Sigma-Aldrich). Cells were scraped and transferred into microcentrifuge tubes, vortexed for 10 minutes, freeze/thawed for 5 cycles, then centrifuged at 12,000 x g for 10 minutes at 4°C, and supernatants were collected. Proteins were separated with TGX 4-20% stain-free polyacrylamide gel (Bio-Rad) in 1x Tris/Glycine/SDS buffer (Bio-Rad) and transferred to 0.2 um nitrocellulose (1620112, Bio-Rad) membrane in 1x Trans-Blot Turbo Transfer Buffer (Bio-Rad) using the Trans-Blot Turbo Transfer System (Bio-Rad) according to the manufacturer recommendations. The membranes were blocked in Odyssey blocking buffer (PBS) (Li-COR) and immunoblotted overnight with primary antibodies against TERT (600-401-252, Rockland), STAT5 (9420S, Cell Signaling), RUNX2 (ab192256, Abcam), MYH11(MAB20221, Abnova), OPN (AF808, R&D systems), αSMA (ab5494, Abcam), TNAP (MAB2909, R&D systems), a-tubulin (926-42213, LI-COR), followed by secondary anti-rabbit or anti-mouse IgG antibody (926-68070, 926-68021, 926-32211, LI-COR). Primary and secondary antibodies were diluted in Odyssey blocking buffer with 0.1% Tween 20. Membranes were washed in PBS with 0.1% Tween 20. Immunofluorescence signals were detected with the Odyssey CLx system (LI-COR), and images were analyzed with Image Studio (Version 5.2, LI-COR).

Immunofluorescent Staining on Fixed Cells

Cells were washed with PBS and then fixed with 4% paraformaldehyde (Electron Microscopy Sciences) for 15 minutes at room temperature, followed by 10 minutes of permeabilization with

TRITON X-100 0.5% (Fisher Scientific). Cells were incubated at room temperature for 1 hour in blocking buffer (PBS, 0.5% Triton-X 100, 5% FBS). Primary antibodies were diluted in the blocking solution and then incubated overnight at 4°C. Next, cells were washed three times for five minutes each with PBS containing 0.1% TWEEN. Fluorescent secondary antibodies were diluted in blocking solution and incubated for one hour protected from the light, then washed three times for five minutes each with PBS, 0.1% TWEEN 20 with a final wash in PBS. Specimens were finally mounted with Fluoroshield Mounting Medium with DAPI (Abcam) and imaged within 24 hours. F-Actin was stained with AlexaFluor488 Phalloidin (Molecular Probes) for 30 minutes, then washed with PBS before mounting. Calcium accumulation was determined with OsteoImage (Lonza) following the manufacturer's recommendations.

Immunofluorescent Staining on Paraffin Sections

Human specimens embedded in paraffin were warmed to 65°C and deparaffinized using xylene and graded alcohol baths, rehydrated in distilled H_2O, and boiled for 20 minutes in antigen unmasking solution (Vector Labs). Cooled samples were then washed with PBS for five minutes. Specimens were then blocked with PBS containing 3% fish skin gelatin and 10% horse serum for one hour. Primary antibodies were diluted in the blocking solution and then incubated overnight at 4°C. Next, specimens were washed three times for five minutes each with PBS containing 3% fish skin gelatin and 0.1% TWEEN 20. Fluorescent secondary antibodies were diluted in a blocking solution and incubated for one hour protected from the light, then washed three times for five minutes each. Specimens were finally mounted with Fluoroshield Mounting Medium with DAPI (Abcam) and imaged within 24 hours.

Alizarin Red Staining and Quantification

Cells were washed with PBS and then fixed with 4% paraformaldehyde (Electron Microscopy Sciences) for 15 minutes at room temperature, followed by two washes with deionized water. Fixed cells were then covered with 40 mM Alizarin Red S (Sigma-Aldrich) at pH 4.1 – 4.3 and gently rocked for 20 minutes at room temperature. Cells were then washed twice with deionized water to remove any unincorporated dye. After imaging, Alizarin Red S was extracted with 10% (v/v) acetic acid (Fisher Scientific) for 30 minutes, scraped into a microcentrifuge tube, vortexed, and then incubated at 85°C for 10 minutes. After chilling on ice for 5 minutes, the mixture was centrifuged at 20,000 x g for 15 minutes at 4°C. 500 µl of supernatant was transferred to a new tube, and 10% (v/v) ammonium hydroxide (Fisher Scientific) was then added to the supernatant. Absorbance was at 405 nm using a 96-well plate spectrophotometer.

Von Kossa Staining

Human specimens embedded in paraffin were warmed to 65°C for one hour and then deparaffinized through xylene and graded alcohol incubations. Specimens were then rehydrated in distilled water. Specimens were stained using the Von Kossa Method of Calcium Kit (Polysciences, 24633-1) following the manufacturer's instructions.

Lentiviral Production and Cell Infection

Lentiviruses were produced by transfecting Dharmacon SMARTvector Lentiviral plasmids encoding shTERT TurboGFP (V3SH11240-225610522) or SMARTvector Non-targeting Control (VSC11707) into HEK293T cells following manufacturer recommendations. The viral-containing supernatant was collected at 48h after transfection, filtered through a 0.45-µm filter, and stored at -80C. Human VICs, CASMCs, and MSCs lines were transduced with MOI of 5 in the presence of 0.8 µg ml^{-1} polybrene (Millipore) to enhance transduction efficiency.

Transcriptional Analysis

Tissue RNA was isolated using Trizol (Life Technologies). Cell RNA was isolated using Quick-RNA MiniPrep (Zymo Research). RNA was treated with DNAse I (Zymo Research) in accordance with the manufacturer's instructions. Reverse transcription was performed using MultiScribe Reverse Transcriptase system (Applied Biosystems). Sixteen ng of cDNA was used per reaction. qPCR was performed on a CFX Connect Real-Time System (Bio-Rad) using PowerUP SYBR Green Master Mix (Applied Biosystems) as follows: one cycle at 95 °C (10 minutes) and 40 cycles of 95 °C (20 seconds) and 58 °C (20 seconds) and 72°C (1 minutes). *GAPDH* or *18s* expression were used to normalize expression. Relative expression was calculated using the average threshold cycle number and the $2^{(Ct(housekeeping\ gene)-Ct(target\ gene))}$ formula. Primers are listed in Supplementary Table 1.

Telomere Length Analysis

Tissue and AVICs genomic DNA was isolated from passage 1 using DirectAmp Tissue Genomic DNA Amplification Kit (Denville Scientific). Telomere length was analyzed using real-time PCR as previously described.[6] Briefly, genomic DNA was isolated following standard protocol, and 10 ng of gDNA per reaction was utilized. Samples were run in triplicate with 35 ng of DNA per reaction, and telomere repeats were amplified using PowerUP SYBR Green Master Mix (Thermofisher Scientific) on a CFX Connect Real-Time PCR System (Bio-Rad). Repeated amplification data were normalized to *RPLP0*/*36b4* as a single copy-gene. Primers are listed in Supplementary Table 1.

Proliferation Assays

Cell proliferation was evaluated using Trypan Blue incorporation in an automatized cell counter Countess II FL (Invitrogen). Briefly, cells were grown on alpha-MEM supplemented with 10% of

FBS and penicillin and streptomycin cocktail (GIBCO) for the duration of the assay. Growth was quantified twice a week. Cell number during OST treatment was determined at the beginning and end of the assay.

Senescence-Associated β-Galactosidase Assays

Cellular senescence was evaluated by senescence-associated β-Galactosidase (SA-β-Gal) activity assay. Briefly, cells were washed with PBS and then fixed with 4% paraformaldehyde (Electron Microscopy Sciences) for 5 minutes at room temperature and then washed twice with PBS. Next, cells were incubated in X-Gal Solution Mix containing 1 mg/mL of 5-Bromo-4-Chloro-3-Indolyl-Alpha-D-Galactopyranoside (American Bioanalytical), 40 mM Sodium Phosphate monobasic solution (Sigma-Aldrich), 40 mM Sodium Phosphate Dibasic solution (Sigma-Aldrich), 40 mM Citric Acid (Sigma-Aldrich), 5 mM Potassium Ferrocyanaide (Sigma-Aldrich), 5 mM Potassium Ferricyanaide (Sigma-Aldrich), 150 mM $NaCl_2$, and 2 mM $MgCl_2$, pH 6.0, for 16 hours at 37°C without CO_2 to develop blue color. Then, cells were washed twice with PBS, and SA-*β*-gal positive cells were imaged and calculated based on randomly selected bright fields areas containing at least 200 cells per field as revelated by subsequent DAPI staining.

Cell Migration Assays

AVICs were seeded in a 12-well plate at a concentration of $1x10^5$ cells per well and were left until they reached 90% of confluence. The well surface was scratched with a 200 µl sterile pipette tip and washed with PBS to remove detached cells. Horizontal lines were drawn on the bottom outside of the well and used as a reference for alignment to obtain the same field for each image acquisition run. VICs media was added, and images were collected at different time points with a phase-contrast microscope using the horizontal lines as reference marks. Scratch

area and scratch width were determined with the Wound Healing Size Macro Tool using ImageJ.[7] Linear regression and two-way ANOVA to compare the changes in the area and the average length of the scratch.

Chromatin Immunoprecipitation

Chromatin Immunoprecipitation (ChIP) was performed on cultured cells as previously described.[8] Briefly, AVICs were stimulated with osteogenic media for 14 days and then collected in 20 mM Na-butyrate dissolved in PBS, and cross-linking of DNA and proteins was performed with formaldehyde (1% vol/vol final concentration) at room temperature. Cross-linking was stopped with 125 mM glycine for 10 min. Cross-linked chromatin was sonicated to obtain fragments between 250 and 750 base pairs in a Bioruptor Pico sonication device (Diagenode). The sheared chromatin was immunoprecipitated with 1 ug of antibody raised against TERT (Rockland, 600-401-252S) and 0.3 ug STAT5 (Cell Signaling, 94205S). Normal rabbit polyclonal IgG (Cell Signaling, 2729S) was used as a negative control. Negative control was incubated with rabbit IgG and input DNA primary antibody. Chromatin complexes were recovered with ChIP-grade Protein G magnetic beads (9006S, Cell Signaling). DNA was recovered with standard phenol-chloroform extraction. Immunoprecipitated DNA was amplified by quantitative RT-PCR using SYBR green. ChIP primers are listed in Supplementary Table 1.

Proximity Ligation Assays (PLA)

PLA was performed directly after cell fixation and according to manufacturer instructions. Briefly, cells were blocked with Duolink blocking solution for 60 minutes at 37°C. Samples were then incubated with rabbit TERT (Rockland) and mouse STAT5 (Santa Cruz) antibodies diluted in Duolink Blocking Solution and incubated overnight at 4°C. Samples were then incubated with secondary antibodies conjugated with PLA probes (DUO92002, DUO92004, Sigma) for 2 h at

37°C in a humidity chamber followed by probe ligation for 30 minutes at 37°C as recommended by the manufacturer. Amplification was performed with Duolink detection kit Red 595 nm for 100 minutes at 37°C (DUO92101, Sigma). Samples were mounted in DAPI-containing mounting media and prepared for image acquisition.

Murine cell isolation

Tert knockout mice (Jackson Labs, 005423) were bred with wild-type mice (Jackson Labs, 000664) to produce *Tert* heterozygous mice, which were then bred to each other to yield *Tert* knockout mice and wild-type littermate controls. Het-het breeding ensures telomeres are intact. Mouse BMMSCs were isolated from femurs and tibias were dissected from three-month-old knockout or wild-type mice. The marrow was rinsed out of the bones with MSC media, and cells were plated and expanded as described previously.[9] Mouse AVICs were isolated from hearts of three-month-old *Tert* knockout or wild-type mice were removed, dissected, and valve leaflet removed. Cells were isolated and expanded as described previously.[10] Mice were given veterinary care by the University of Pittsburgh Division of Laboratory Animal Resources, which adheres to the NIH policy on the Animal Welfare Act and all other applicable laws. Facilities are under the full-time supervision of veterinarians and are AAALAC-accredited. Our protocols follow the AVMA Guidelines on Euthanasia. All animal breeding and isolations were approved by the Institutional Animal Care and Use Committee at the University of Pittsburgh. We made attempts to minimize the number of mice required to complete experiments.

Promoter Analysis

The upstream region of the *RUNX2* (NM_001015051.3) promoter was scanned with LASAGNA[11] and TRANSFAC/MATCH[12] suites. Searches were carried out with data version 2021.3, high

quality matrices and cut off to minimize false positives hits. STAT5 logo analysis was performed with WebLogo (weblogo.berkeley.edu).

Statistics

Statistical analyses were performed with GraphPad Prism 9.2 (GraphPad Software, San Diego, CA) software. All experiments used at least n = 3 biological replicates and were run in technical duplicates. Statistical comparisons between the two groups were performed by a nonparametric Mann-Whitney *U* test. Statistical comparisons among more than two groups were performed by nonparametric Kruskal-Wallis *H* tests with post hoc Dunn's multiple pairwise comparisons between groups or by Two-way ANOVA. Shapiro-Wilk normality test was used. to test data distribution. Data are presented as mean ± standard deviation (SD).

REFERENCES

1. Cuevas RA, Chu CC, Moorhead Iii WJ, Wong R, Sultan I, St. Hilaire C. Isolation of Human Primary Valve Cells for In vitro Disease Modeling. *JoVE*. 2021:e62439. doi: doi:10.3791/62439
2. Cuevas RA, Chu CC, Moorhead WJ, 3rd, Wong R, Sultan I, St Hilaire C. Isolation of Human Primary Valve Cells for In vitro Disease Modeling. *J Vis Exp*. 2021:e62439. doi: 10.3791/62439
3. Gupta GK, Dhar K, Del Core MG, Hunter WJ, 3rd, Hatzoudis GI, Agrawal DK. Suppressor of cytokine signaling-3 and intimal hyperplasia in porcine coronary arteries following coronary intervention. *Exp Mol Pathol*. 2011;91:346-352. doi: 10.1016/j.yexmp.2011.04.004
4. Hoemann CD, El-Gabalawy H, McKee MD. In vitro osteogenesis assays: influence of the primary cell source on alkaline phosphatase activity and mineralization. *Pathol Biol (Paris)*. 2009;57:318-323. doi: 10.1016/j.patbio.2008.06.004
5. Pascolo E, Wenz C, Lingner J, Hauel N, Priepke H, Kauffmann I, Garin-Chesa P, Rettig WJ, Damm K, Schnapp A. Mechanism of human telomerase inhibition by BIBR1532, a

synthetic, non-nucleosidic drug candidate. *J Biol Chem*. 2002;277:15566-15572. doi: 10.1074/jbc.M201266200

6. Cawthon RM. Telomere measurement by quantitative PCR. *Nucleic Acids Res*. 2002;30:e47. doi: 10.1093/nar/30.10.e47

7. Suarez-Arnedo A, Torres Figueroa F, Clavijo C, Arbelaez P, Cruz JC, Munoz-Camargo C. An image J plugin for the high throughput image analysis of in vitro scratch wound healing assays. *PLoS One*. 2020;15:e0232565. doi: 10.1371/journal.pone.0232565

8. Dahl JA, Collas P. A rapid micro chromatin immunoprecipitation assay (microChIP). *Nat Protoc*. 2008;3:1032-1045. doi: 10.1038/nprot.2008.68

9. Huang S, Xu L, Sun Y, Wu T, Wang K, Li G. An improved protocol for isolation and culture of mesenchymal stem cells from mouse bone marrow. *J Orthop Translat*. 2015;3:26-33. doi: 10.1016/j.jot.2014.07.005

10. Bouchareb R, Lebeche D. Isolation of Mouse Interstitial Valve Cells to Study the Calcification of the Aortic Valve In Vitro. *J Vis Exp*. 2021. doi: 10.3791/62419

11. Lee C, Huang CH. LASAGNA: a novel algorithm for transcription factor binding site alignment. *BMC Bioinformatics*. 2013;14:108. doi: 10.1186/1471-2105-14-108

12. Wingender E, Dietze P, Karas H, Knuppel R. TRANSFAC: a database on transcription factors and their DNA binding sites. *Nucleic Acids Res*. 1996;24:238-241. doi: 10.1093/nar/24.1.238

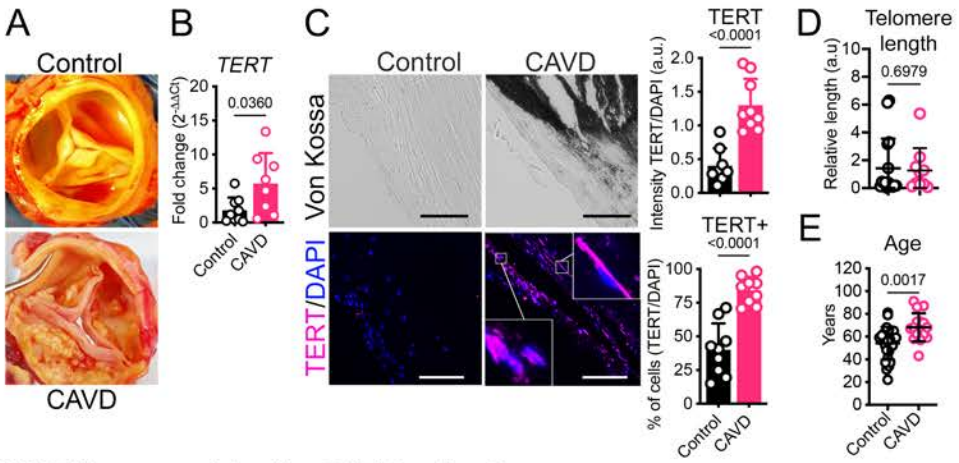

Figure 1. TERT is upregulated in CAVD valve tissue.

A, Surgically removed specimen of control (top) and CAVD (bottom) human valves. B, TERT mRNA transcript quantification in control and CAVD valve tissues. n = 8 control, n= 9 CAVD. C, Representative serial sections of Von Kossa (dark precipitation, top panels) and TERT immunofluorescent staining (bottom panels) in control and CAVD valve tissues. Scalebar 100 µm. Quantification of TERT intensity and the number of TERT-positive cells on the leaflet is shown on the right graphs. n = 9 control, n = 9 CAVD. D, Telomere length measurements in valve tissues. n = 16 control, n = 10 CAVD. E. Age of the patients utilized in this study. n = 25 control, n = 16 CAVD. Data are shown as means ± SD. *P* values were calculated by the Mann-Whitney *U* test and shown on each graph.

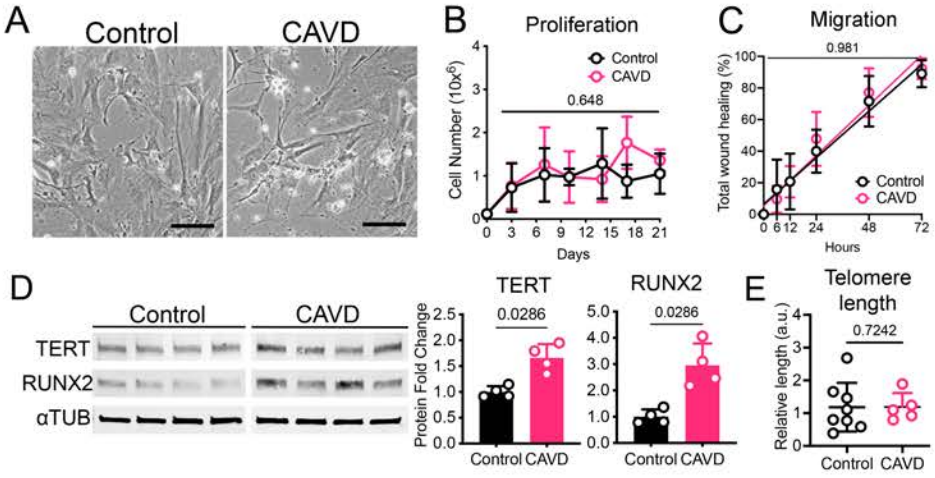

Figure 2. Valve interstitial cells isolated from CAVD patients show elevated TERT expression at baseline.

A, Representative images showing cell morphology of control (left) and CAVD (right) VICs. Scalebar 50 μm. B, Proliferation of control and CAVD VICs at baseline. n = 3 control, n = 3 CAVD. Data represents means ± SD. C, Relative migration distances of control and CAVD VICs. n = 10 control, n = 10 CAVD. Representative western blot staining of control and CAVD VICs at baseline. Quantification of protein levels is shown on the right panels. n = 4 control, n = 4 CAVD/. E, Telomere length measurements in VICs. n = 8, control, n = 5 CAVD; means ± SD. Data are shown as means ± SD. *P* values were calculated by the Mann-Whitney *U* test and shown on each graph.

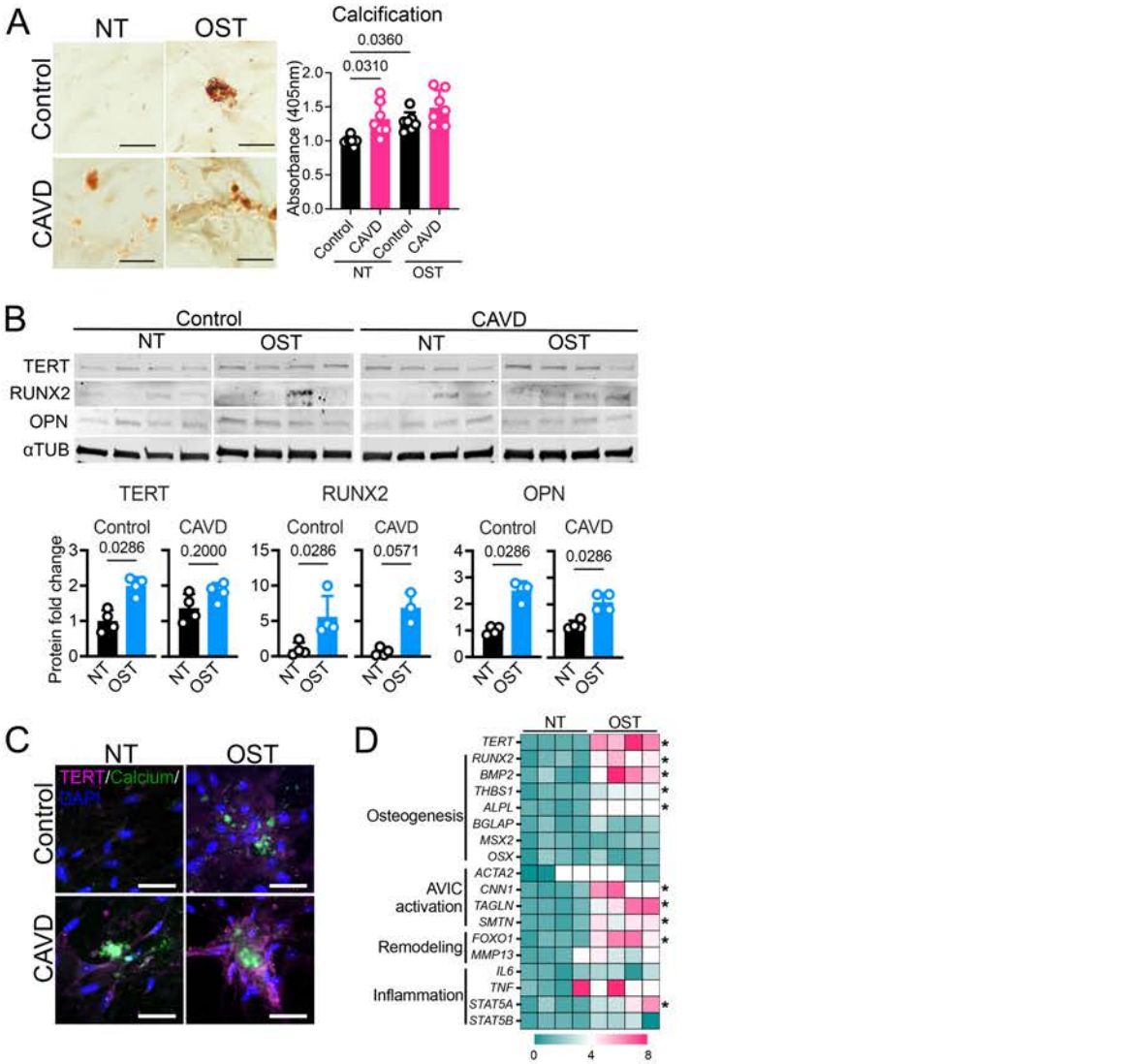

Figure 3. TERT is upregulated during osteogenic differentiation of VICs.
A, Representative images of VICs growing in normal conditions (no treatment, NT, left panel) or stimulated with osteogenic media (OST) for 14 days. Calcium deposition was visualized by Alizarin Red staining. Scalebar 50 μm. Quantification of calcification is shown as average absorbance ± SD on the right graphs. n = 7 control, n = 7 CAVD. B, Representative western blot staining of samples from control and CAVD VICs after 14 days of NT or OST. Quantification of protein levels is shown on the right graphs. n = 4 control, n = 4 CAVD. C, Representative immunofluorescent staining images of TERT in control and CAVD VICs after 14 days of NT or OST. Calcium deposition was visualized by OsteoImage staining. Scalebar 100 μm. D. Expression profile control VICs after 14 days of NT and OST treatment. n = 4 NT, n = 4 OST. Data are shown as means ± SD. *P* values were calculated by the Mann-Whitney *U* test with * *P* = 0.0286 in Figure D.

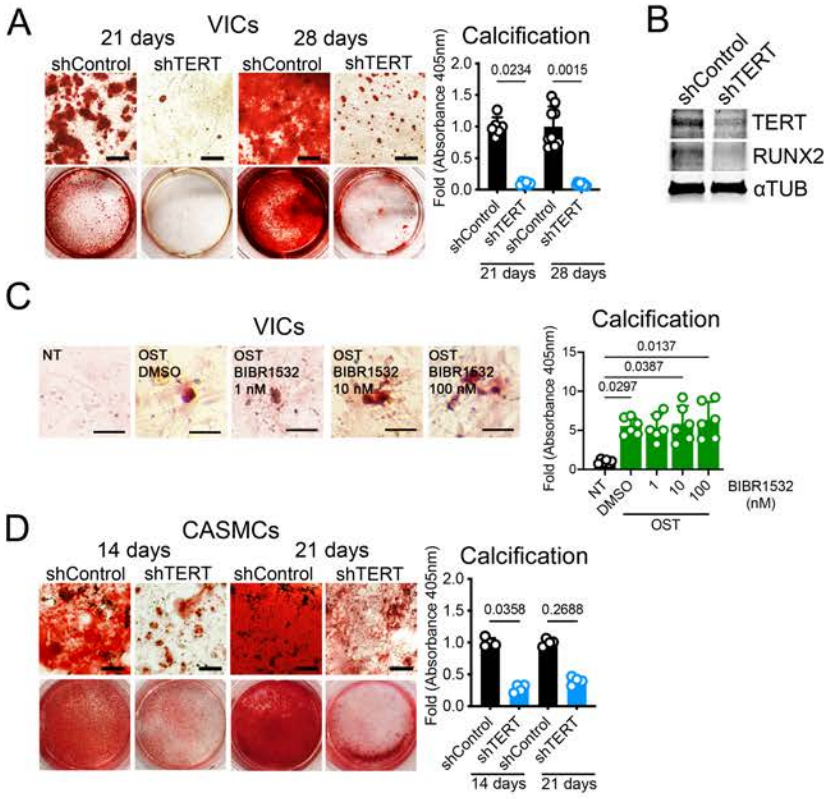

Figure 4. TERT is required for osteogenic transition and calcification of human cells.
A, VICs transduced with lentivirus containing either short hairpin scramble (shControl-GFP) or short hairpin TERT (shTERT-GFP) and followed by OST stimulated for up to 28 days. Calcium deposition was visualized by Alizarin Red staining. Quantification of calcification is presented as average absorbance on the right graph. n = 6 shControl, n = 6 shTERT at 21 days and n = 9 shControl, n = 9 shTERT at day 28. Scalebar 400 μm. Data are shown as means ± SD.
B, Representative western blot staining of VICs transduced with lentivirus containing either shControl-GFP or shTERT-GFP followed by 7 days of osteogenic stimulation. C. VICs treated with BIBR1532 and stimulated with osteogenic media for 28 days. Scalebar 50 μm. Quantification of calcification is shown on the right graph. n = 6. Data are shown as means ± SD. D, CASMCs transduced with lentivirus containing either shControl-GFP or shTERT-GFP and stimulated with osteogenic media for up to 21 days. n = 4 shControl, n = 4 shTERT for both time points. Scalebar 400 μm. Quantification of calcification is shown on right graph. *P* values were calculated with the Kruskal-Wallis *H* test with Dunn post hoc test and shown on top of each graph.

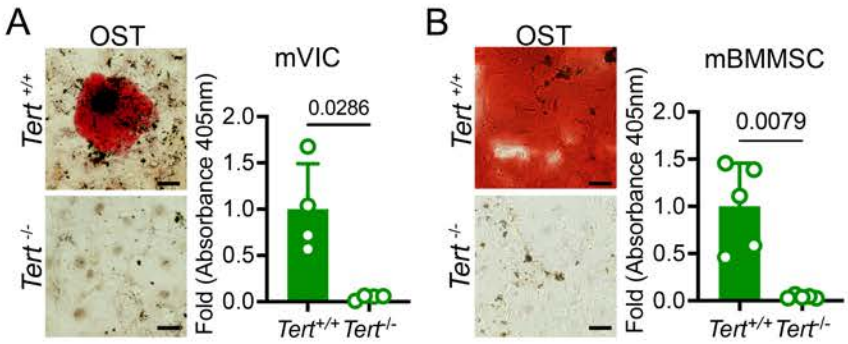

Figure 5. TERT is required for the osteogenic transition of murine cells.
A, Representative images of mVICs isolated from wild-type (*Tert* $^{+/+}$) or F1 *Tert* knockout (*Tert* $^{-/-}$) mice and stimulated with osteogenic media for 21 days. Scalebar 100 μm. Quantification of calcification is shown on the right graph. B, Representative images of mBMMSCs isolated from *Tert* $^{+/+}$ or *Tert* $^{-/-}$ mice and stimulated with osteogenic media for 21 days. Scalebar 100 μm. Quantification of calcification is presented as average absorbance on the right graphs. All graphs are n = 4 *Tert* $^{+/+}$, n = 4 *Tert* $^{-/-}$. Data are shown as means ± SD. *P* values were calculated by the Mann-Whitney *U* test and indicated on each graph.

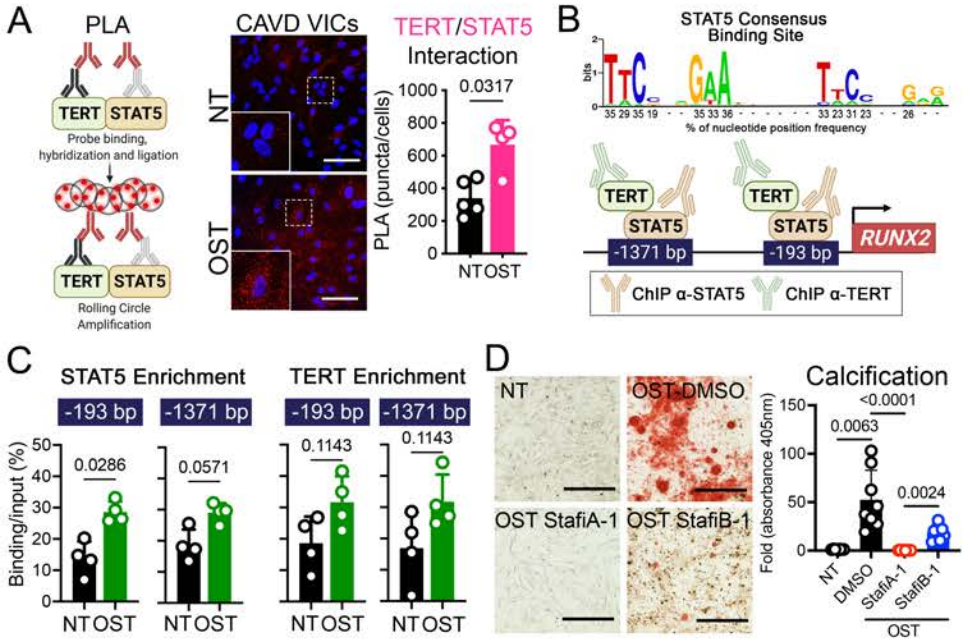

Figure 6. TERT and STAT5 interact to upregulate RUNX2 expression in human VICs. A, Diagram of proximity ligation assay (PLA, left panel). Representative images of TERT/STAT5 complex (red foci) in CAVD VICs cultured for 21 days in osteogenic medium and detected by PLA. Scalebar 100 μm (middle panel). Quantification of PLA signal is shown in the right graph. n = 4. B, Logo analysis depicting the consensus binding site for tetrameric STAT5 (top panel). Diagram depicting STAT5 and TERT binding RUNX2 promoter and the positions of the predicted STAT5 binding sites (bottom panel). C, STAT5 (left graphs) and TERT (right graphs) enrichment on the RUNX2 promoter of control VICs after 14 days of osteogenic stimulation and quantified by ChIP-qPCR. n = 4. D, Representative images of control and CAVD VICs treated with 10 μM of the STAT5 inhibitors StafiA-1or StafiB-1 during 28 days of osteogenic stimulation. Scalebar 400 μm. n = 8, means ± SD. Quantification of calcification is shown on the right graph. Data are shown as means ± SD. P values were calculated by the Mann-Whitney U test (Figure A and C) and Kruskal-Wallis H test (Figure D) and indicated on each graph.

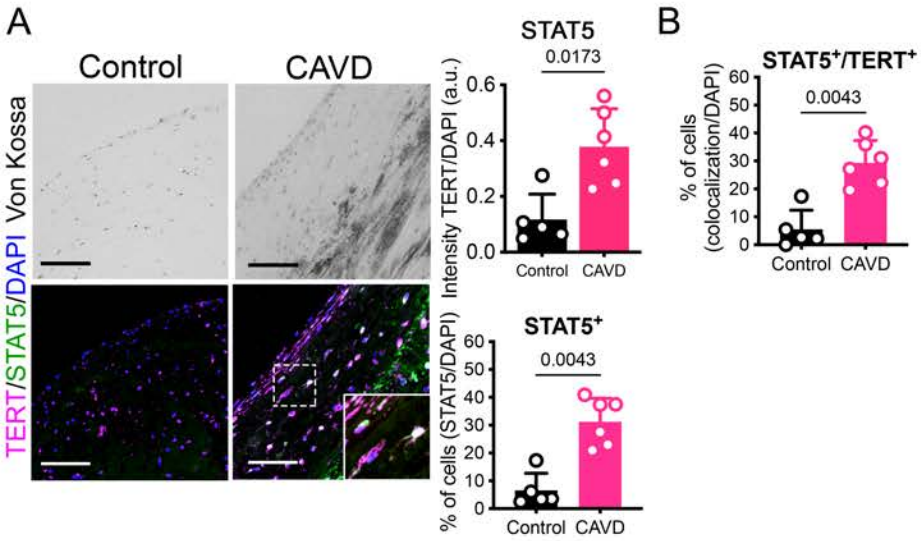

Figure 7. TERT and STAT5 are upregulated and colocalize in CAVD tissue.
A, Representative serial sections of Von Kossa (dark precipitation, top panels) and TERT and STAT5 immunofluorescent staining (bottom panels) in control and CAVD valve tissues. Scalebar 100 µm. Quantification of STAT5 intensity and STAT5-positive cells (STAT5+) are shown on the right panels. B, Quantification of STAT5-TERT-positive cells. Data are shown as means ± SD, n = 5 control, n = 6 CAVD. *P* values were calculated with the Mann-Whitney *U* test and indicated on each graph.

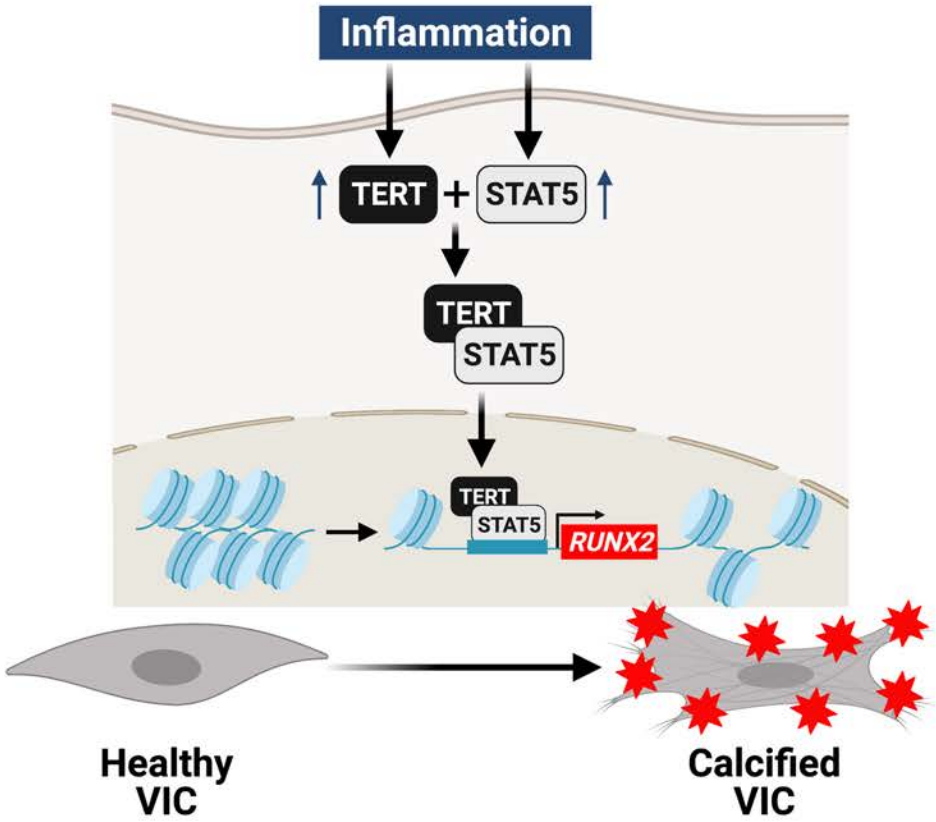

Figure 8. TERT/STAT5 promotes osteogenic reprogramming
Inflammation promotes the upregulation and interaction of TERT and STAT5. Then, the TERT/STAT5 complex translocates into the nucleus where TERT facilitates STAT5 binding to the promoter region of *RUNX2* gene, to engage the osteogenic reprogramming of VICs during the early stages of CAVD pathogenesis.

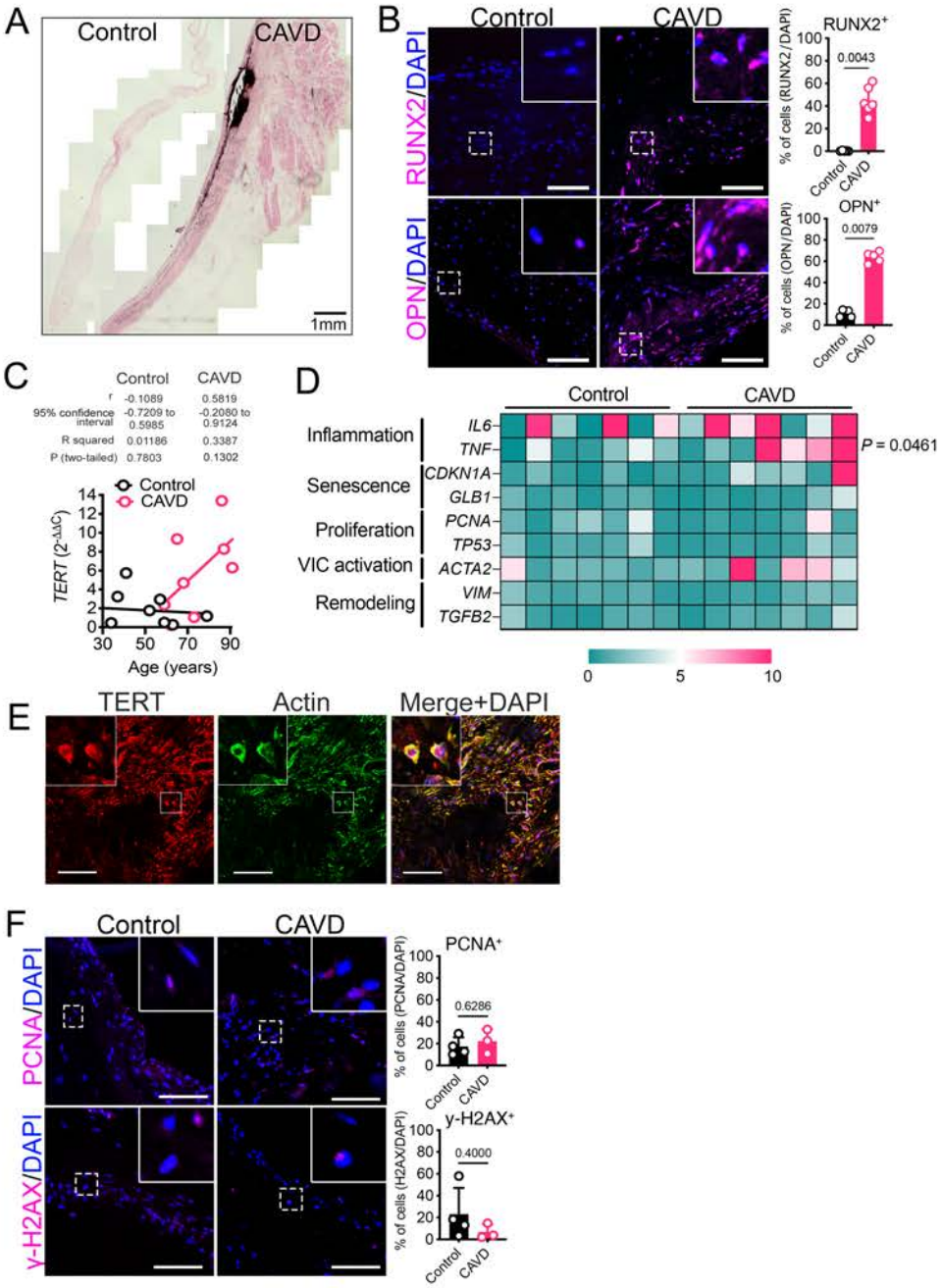

Supplemental Figure 1. Characterization of human CAVD valves and correlation of TERT expression with age.

A, Representative section of Von Kossa staining in control and valve CAVD leaflets tissue. Scalebar 1 mm. B, Representative serial sections of RUNX2 immunofluorescent staining (top panels) and OPN (bottom panels) in control and CAVD valve tissues. Scalebar 100 μm. Quantification of RUNX2-positive cells and OPN-positive cells on the leaflet specimen is shown on the right graphs. n = 5 control, n = 6 CAVD. C, Correlation between age of the donor and *TERT* expression. n = 8 control, n = 9 CAVD, Pearson correlation test. D, Expression profile in the subject leaflets. n = 7 control, n = 7 CAVD. E, Confocal images of a CAVD leaflet. Scalebar 50 μm. F, Representative images of immunofluorescent staining of PCNA (top panels) and γ-H2AX (bottom panels) in control and CAVD valve tissues. Scalebar 100 μm. Quantification of PCNA-positive cells and γ-H2AX-positive cells are shown on the right graphs. n = 4 control, n = 3 CAVD. Data are showns as means ± SD. *P* values were calculated with the Mann-Whitney *U* test (Figures B, G, and F) and two-way ANOVA with Sidak post hoc test (heatmap on D).

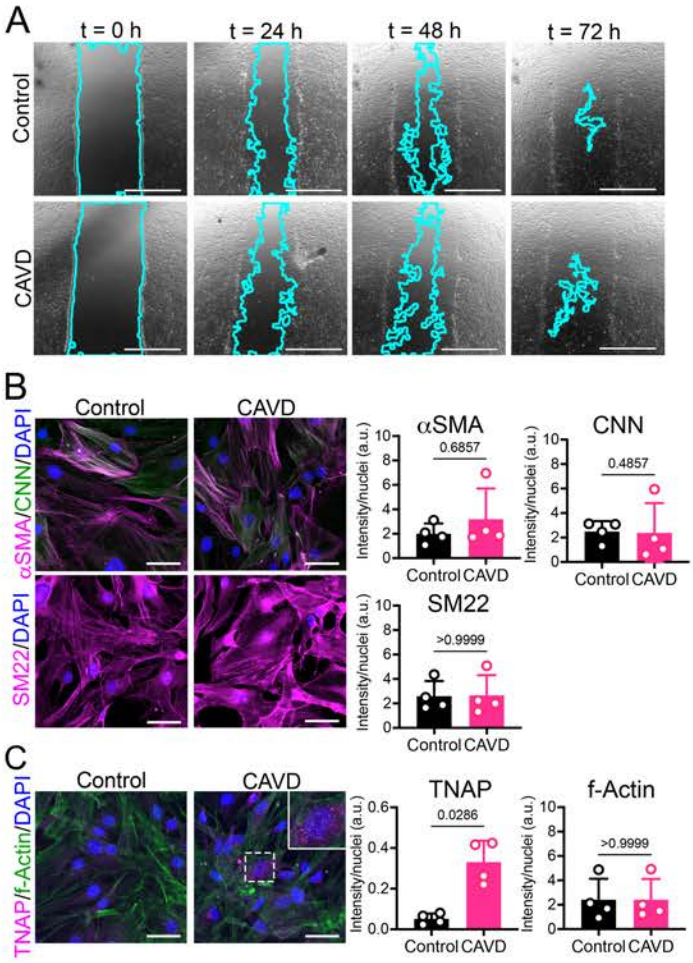

Supplemental Figure 2. VIC migration, activation, and osteogenic markers at baseline. A, Representative images of a scratch assay in control (top panels) and CAVD (bottom panels) VICs. Time points are indicated on top of each panel. Blue lines denote the cell migration front. Scalebar 1 mm. n = 10 control, n = 10 CAVD. B, Representative images of αSMA and CNN (top panels) and SM22 (bottom panels) in control and CAVD VICs. Scalebar 50 μm. Signal quantification of αSMA, CNN, and SM22 are shown on the right panels. n = 4 control, n = 4 CAVD. C, Representative images of TNAP and f-Actin signal in control and CAVD VICs. Scalebar 50 μm. Signal quantification of TNAP and f-Actin is shown on the right panels. n = 4 control, n = 4 CAVD. Data are shown as means ± SD. *P* values were calculated with the Mann-Whitney *U* test and shown on top of each graph.

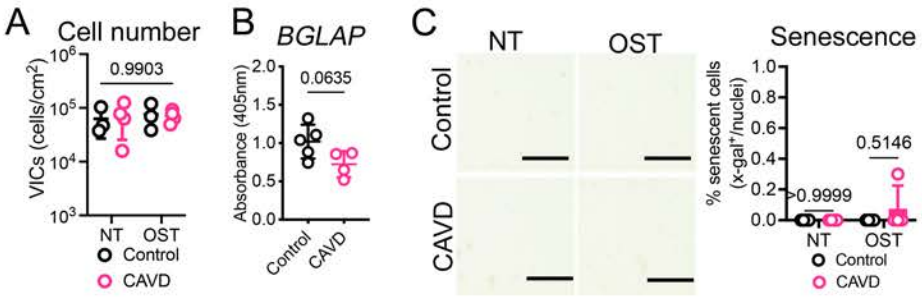

Supplemental Figure 3. Senescence is not operative during the osteogenic differentiation of VICs.

A, Cell counting of control and CAVD VICs after 14 days of NT or OST stimulation. n = 4 control, n = 4 CAVD. B, β-galactosidase (*BGLAP*) mRNA transcript quantification in control and CAVD VICs at baseline. n = 5 control, n= 4 CAVD. C, Representative images of senescence-associated β-galactosidase activity staining of VICs after 28 days of NT or OST stimulation. Blue cells were considered positive for senescence. Quantification of senescence is shown on the right graph. n = 4 control; n = 4 CAVD. Data are shown as means ± SD. *P* values were calculated with the Mann-Whitney U test (figure A and B) and the Kruskal-Wallis *H* test with Dunn post hoc test and shown on top of each graph.

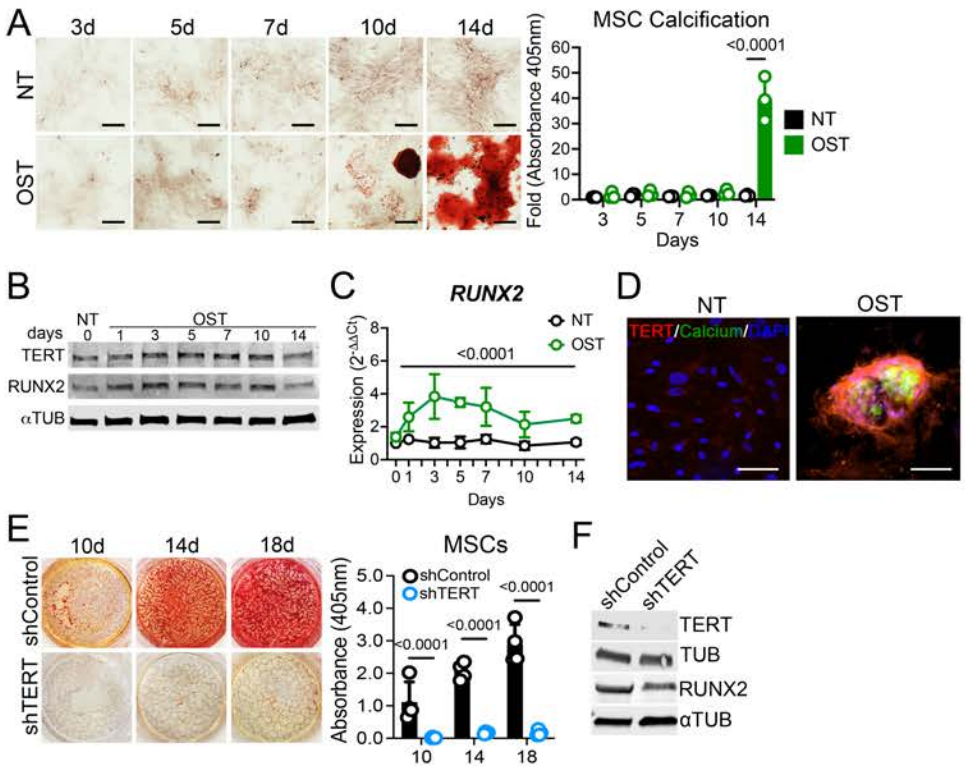

Supplemental Figure 4. TERT is upregulated and required for the osteogenic differentiation of human mesenchymal stem cells.

A, Representative images of human MSCs stimulated with OST for 14 days. Calcium deposition was visualized by Alizarin Red staining. Quantification of calcification is shown on the right graph. n = 3. Scalebar 50 μm. B, Western blot staining of samples from MSCs collected during the 14 days of OST treatment. C, TERT and RUNX2 expression profile of differentiating MSCs stimulated for 14 days with OST media. n = 3. D, Representative TERT immunofluorescent staining images of MSCs stimulated with osteogenic media for 14 days. Scalebar 100 μm. E, MSCs transduced with lentivirus containing either shControl-GFP or shTERT-GFP and stimulated with osteogenic media for up to 21 days. Quantification of calcification is shown on the right graph. n = 4; means ± SD. F, Representative western blot staining of MSCs transduced with lentivirus containing either shControl-GFP or shTERT-GFP followed by 7 days of osteogenic stimulation. Data are shown as means ± SD. *P* values were calculated by Kruskal-Wallis *H* test with Dunn pairwise comparison post hoc test (Figure C) and two-way ANOVA with Tukey post hoc test (Figures A and E).

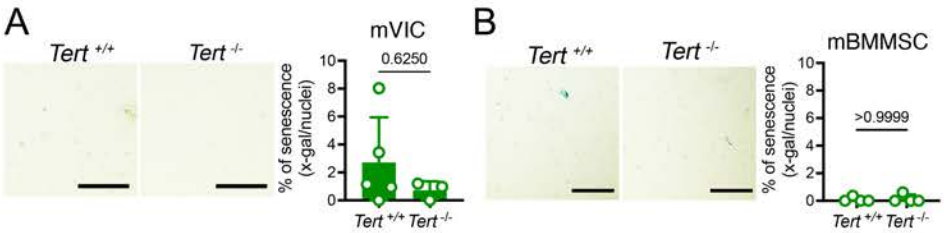

Supplemental Figure 5. Senescence is not operative in mice *Tert* $^{-/-}$ cells.
A, Representative images of a senescence-associated β-galactosidase (SA-β-gal) staining of mVICs isolated from wild-type (*Tert* $^{+/+}$) or F1 *Tert* knockout (*Tert* $^{-/-}$) mice after 21 days of OST stimulation. Blue cells were considered positive for senescence. Quantification of senescence cells is shown on the right graph. B, Representative images of SA-β-gal staining of mBMMSCs isolated from *Tert* $^{+/+}$ or *Tert* $^{-/-}$ mice after 21 days of osteogenic stimulation. Blue cells were considered to be positive for senescence. Quantification of senescence is shown on the right graph. Both figures, n = 5 *Tert* $^{+/+}$, n = 3 *Tert* $^{-/-}$. Scalebar 400 μm. Data are shown as means ± SD and *P* were calculated with the Mann-Whitney *U* test and shown on each graph.

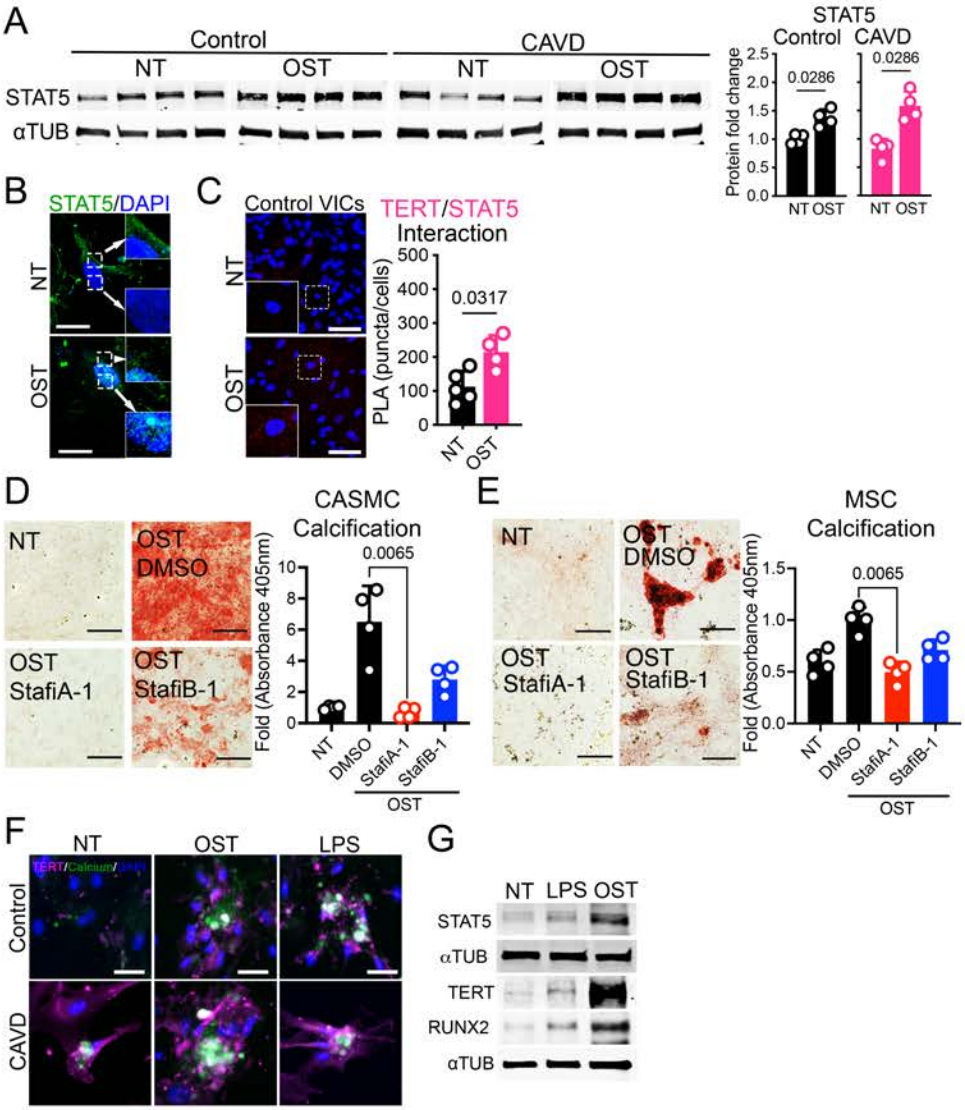

Supplemental Data Fig 6. STAT5 is upregulated and required during osteogenic differentiation of VICs.

A, Representative western blot staining of samples from CAVD and control VICs after 14 days of OST stimulation. Quantification of protein levels is shown on the right graphs. n = 4, control n = 4 CAVD. B, Representative immunofluorescence image of STAT5 shows subcellular distribution after 14 days of NT and OST stimulation. Scalebar 40 µm. C, Representative images of TERT/STAT5 complex (red foci) in control VICs and detected by proximity ligation assay (PLA). Scalebar 100 µm. Quantification of PLA is shown on the right graph. n = 4. D, Representative images of CASMCs (left panels) treated with 10 µM of the STAT5 inhibitors StafiA-1 or StafiB-1 during the 14 days of OST stimulation. Scalebar 400 µm. Quantification of calcification is shown on the right graph. n = 4. E, Representative images of MSCs (left panels) treated with 10 µM of the STAT5 inhibitors StafiA-1 or StafiB-1 during the 21 days of OST stimulation. Scalebar 400 µm. Quantification of calcification is shown on the right graph. n = 4. F, Representative immunofluorescence images of VICs after 14 days of LPS treatment or OST stimulation. Scalebar 50 µm. G, Representative western blot staining of CAVD VICs after 14 days of OST stimulation. Data are shown as means ± SD. *P* values were calculated with the Mann-Whitney *U* test (Figures A and B) and the Kruskal-Wallis *H* test with Dunn pairwise comparison post-test (Figured D and E) and indicated in each graph.

Table 1: Patient information

Patient ID	Age	Sex	Cause of Death	Calcification (Von Kossa Staining)	Hypertension	Diabetes	Smoking	Alcohol
2016-037	31	Male	Brain anoxia due to cardiovascular complications	No	No	No	Unknown	Yes
2016-038	81	Male	Myocardial Infarction	No	No	No	Unknown	Unknown
2016-042	22	Female	Brain anoxia due to head trauma	No	No	No	No	Unknown
2016-045	59	Female	Stroke	No	PH	Yes	Yes	Unknown
2016-046	65	Male	Head trauma from accident	No	No	No	Unknown	Unknown
2016-048	56	Female	Stroke	No	HTN	No	Unknown	Unknown
2016-050	65	Male	Stroke	No	HTN	No	Unknown	Yes
2016-054	63	Female	Hemorriage and Ruptire AAA	No	No	Yes	No	Unknown
2016-065	58	Male	Stroke	No	HTN	Yes	Yes	Unknown
2016-073	41	Female	Traumatic arrest and motor vehicle accident	No	HTN	No	Yes	Unknown
2016-078	34	Female	Heart Failure	No	No	No	Unknown	Unknown
2016-079	59	Male	Respiratory failure	No	HTN	No	No	Unknown
2016-083	52	Male	Stroke	No	PAH	No	Yes	Unknown
2016-085	52	Male	Myocardial Infarction	No	PH	No	Unknown	Unknown
2016-091	59	Female	Stroke	No	HTN	No	Unknown	Unknown
2016-092	47	Female	Stroke	No	No	No	No	Unknown
2016-098	57	Male	Cardiac arrest	No	HTN	No	Yes	Unknown
2016-101	37	Female	Cardiac Death	No	No	No	Unknown	Unknown
2016-146	79	Male	Cardiac arrest	No	No	No	Yes	Unknown
2017-005	66	Female	Stroke	No	No	No	Unknown	Unknown
2017-035	48	Female	Brain anoxia due to CO poisoning	No	No	No	Unknown	Unknown
2017-051	56	Male	Brain anoxia due to cardiac arrest	No	No	No	Unknown	Unknown
2017-069	37	Male	Motor vehicle accident	No	No	No	Unknown	Unknown
03-0127	61	Male	Surgical replacement due to aortic reconstruction for aneurysm	No	HTN	No	Unknown	Unknown
03-0129	68	Male	Surgical replacement due to aortic reconstruction for aneurysm	No	HTN	Yes Type II	Unknown	Unknown
2016-034	91	Male	Natural causes	Yes	No	No	No	Unknown
2016-051	65	Male	Natural causes	Yes	HTN	No	Yes	Yes
2016-053	73	Male	Congestive heart failure	Yes	No	No	No	Unknown

2016-060	73	Male	Cardiac arrest	Yes	No	No	Unknown	Unknown
2016-061	67	Male	Natural causes	Yes	No	Yes	Unknown	Unknown
2016-062	59	Male	Cardiac arrest	Yes	No	No	Yes	Unknown
2016-068	68	Female	Intracranial hemorrhage	Yes	No	No	Yes	Unknown
2016-072	62	Female	Cardiac arrest	Yes	No	No	No	Unknown
2016-093	43	Male	Cardiac arrest	Yes	HTN	Yes	No	Unknown
2016-095	87	Male	Myocardial Infarction	Yes	HTN	No	Yes	Unknown
2016-102	58	Female	Cardiac arrest and asystole	Yes	No	No	Yes	Unknown
2016-103	72	Male	Cardiac arrest	Yes	HTN	No	Unknown	Unknown
2016-105	86	Male	Cardiac arrest	Yes	No	No	No	Unknown
2016-118	62	Male	Cardiac arrest	Yes	No	No	No	Unknown
2017-025	57	Female	Brain anoxia due to choking	Yes	No	Yes Type II	Unknown	Unknown
2017-076	68	Female	Myocardial Infarction	Yes	No	No	No	Unknown

HTN = Hypertension PH = Pulmonary Hypertension PAH = Pulmonary Arterial Hypertension

Table 2: Patient Summary

Summary	total	age	% male	% hypertension	% CVD death	% deceased
control	25	54	52%	48%	68%	100%%
calcified	16	68	81%	25%	81%	100%

Supplemental Table 1: TRANSFAC STAT5 Binding Sites on RUNX2 promoter

Transcription Factor	Position	Core score	Matrix score	Sequence
STAT5A (homodimer)	-4571	1	0.948	ctTTTCCaagaaagc
STAT5B (homodimer)	-4571	0.968	0.954	cttttccaAGAAAgc
STAT5B:STAT5A	-4570	1	0.999	ttTTCCAagaa
STAT5A	-4570	1	0.994	ttttccAAGAAag
STAT5A	-4568	1	1	TTCCAagaaa
STAT5A (homotetramer)	-4568	0.996	0.846	ttccaAGAAAgctaatatacaaaa
STAT5A	-3801	1	1	tAGAAAtg
STAT5A	-3035	1	1	tAGAAAtg
STAT5A (homotetramer)	-2843	0.996	0.866	taccaacaacttttTTTCTttgaa
STAT5A (homotetramer)	-2828	0.977	0.899	ttcttTGAAAttgatttcaagatc
STAT5A (homotetramer)	-2875	0.977	0.873	gggtttgtaagatgTTTCAgtgaa
STAT5A (homotetramer)	-1371	0.788	0.834	taaatggcaaaaaaATGCCtagaa
STAT5A (homotetramer)	-193	0.995	0.882	tgccaGGAAAggccttaccacaag

Supplementary Table 2: Primers

Species	Gene	Forward Primer Sequence 5' -> 3'	Reverse Primer Sequence 5' -> 3'	Techniq	Source
Human	TERT	GCATTGGAATCAGACAGCAC	CCACGACGTAGTCCATGTTC	qPCR	Sigma-Aldrich
Human	RUNX2	ATTCCTGTAGATCCGAGCACC	GCTCACGTCGCTCATTTTGC	qPCR	IDT
Human	MSX2	GAGCTGGGATGTGGTAAAGG	AAATTCAGAAGATGGAGCGG	qPCR	IDT
Human	CDKN1A	TGTCCGTCAGAACCCATG	AAAGTCGAAGTTCCATCGCTC	qPCR	IDT
Human	PCNA	ACACTAAGGGCCGAAGATAAC	ACAGCATCTCCAATATGGCTGA	qPCR	IDT
Human	TP53	GAGGTTGGCTCTGACTGTACC	TCCGTCCCAGTAGATTACCAC	qPCR	IDT
Human	ALPL	ATGGGATGGGTGTCTCCACA	CCACGAAGGGGAACTTGTC	qPCR	IDT
Human	GLB1	TATACTGGCTGGCTAGATCACTG	GGCAAAATTGGTCCCACCTATAA	qPCR	IDT
Human	STAT3	CAGCAGCTTGACACACGGTA	GCCCAATCTTGACTCTCAATCC	qPCR	IDT
Human	STAT5A	ATGTGAAACCACAGATCAAG	TCTGTGGGTACATGTTATAGG	qPCR	Sigma-Aldrich
Human	STAT5B	ATGGGACTCAGTAGATCTTG	CTTCAGTAAAAACCCATCTTCC	qPCR	Sigma-Aldrich
Human	TGFb2	CTGCATCTGGTCACGGTCG	CCTCGGGCTCAGGATAGTCT	qPCR	IDT
Human	OSX	CCCCCTTTACAAGCACTAATGG	GGCAGACAGTCAGAAGAGCTG	qPCR	IDT
Human	ACTA2	AAAAGACAGCTACGTGGGTGA	GCCATGTTCTATCGGGTACTTC	qPCR	IDT
Human	FOXO1	TCGTCATAATCTGTCCCTACACA	CGGCTTCGGCTCTTAGCAAA	qPCR	Sigma-Aldrich
Human	18s	GTAACCCGTTGAACCCCATT	CCATCCAATCGGTAGTAGCG	qPCR	IDT
Human	MYH11	CGCCAAGAGACTCGTCTGG	TCTTTCCCAACCGTGACCTTC	qPCR	IDT
Human	IL6	AAATTCGGTACATCCTCGACGG	GGAAGGTTCAGGTTGTTTTCTGC	qPCR	IDT
Human	VIM	GGAAACTAATCTGGATTCACTC	CATCTCTAGTTTCAACCGTC	qPCR	Sigma-Aldrich
Human	SOX9	GCCAGGTGCTCAAAGGCTA	TCTCGTTCAGAAGTCTCCAGAG	qPCR	IDT
Human	KLF4	CCCACATGAAGCGACTTCCC	CAGGTCCAGGAGATCGTTGAA	qPCR	IDT
Human	SM22	AGTGCAGTCCAAAATCGAGAAG	CTTGCTCAGAATCACGCCAT	qPCR	IDT
Human	TNF	CCTCTCTCTAATCAGCCCTCTG	GAGGACCTGGGAGTAGATGAG	qPCR	IDT
Human	BGLAP	GGACTGTGACGAGTTGGCTG	CCGTAGAAGCGCCGATAGG	qPCR	IDT
Human	SMTN	CAAAAAGTCCTAACCCCTGCT	TCATGTCGTCCACCTCCAC	qPCR	IDT
Human	BMP2	ACCCGCTGTCTTCTAGCGT	TAAATTGAAGAAGAAGCGCC	qPCR	Sigma-Aldrich
Human	THBS1	TGCTCCAATGCCACAGTTCC	CTGCTGAATTCCATTGCCACA	qPCR	IDT
Human	CNN1	GTCAACCCAAAATTGGCACCA	ACCTTGTTTCCTTTCGTCTTCG	qPCR	IDT
Human	MMP13	CACCAATTCCTGGGAAGTCT	GCAGCTGTTCACTTTGAGGA	qPCR	IDT
Human	GAPDH	CTGGGCTACACTGAGCACC	AAGTGGTCGTTGAGGGCAATG	qPCR	IDT
Human	pRUNX2-1	ACCTTACAGGAGTTTGGGCT	CTTTCCTGGCATCCAGAAGGATA	ChIP	IDT
Human	pRUNX2-2	CCGCCCACCCCATTTACTT	GGCGAACAGACCAATTTTCTAGG	ChIP	IDT
Human	hTelomere	GGTTTTTGAGGGTGAGGGTGAGGGT	TCCCGACTATCCCTATCCCTATCCCT	PCR	Sigma-Aldrich